FLOW INTERFERENCE BETWEEN TWO CIRCULAR CYLINDERS AT DIFFERENT ARRANGEMENTS

by
MEENU KAPIL

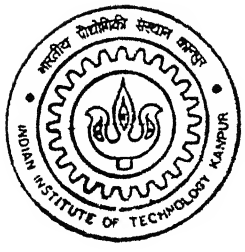

DEPARTMENT OF AEROSPACE ENGINEERING
INDIAN INSTITUTE OF TECHNOLOGY, KANPUR
August, 2000

FLOW INTERFERENCE BETWEEN TWO CIRCULAR CYLINDERS AT DIFFERENT ARRANGEMENTS

A Thesis Submitted
in Partial Fulfillment of the Requirements
for the Degree of

Master of Technology

by

MEENU KAPIL

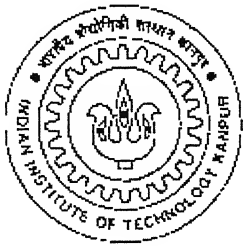

to the

DEPARTMENT OF AEROSPACE ENGINEERING
INDIAN INSTITUTE OF TECHNOLOGY
KANPUR 208016

AUGUST 2000

CERTIFICATE

It is certified that the work presented in this thesis entitled **"Interference Between Two Circular Cylinders at Different Arrangements"** has been carried out under my supervision in partial fulfillment of the requirements for the award of M.Tech. Degree in Aerospace Engineering. This thesis is a record of bonafide work carried out in the Department of Aerospace Engineering, I.I.T. Kanpur during the year 1999-2000 and this work has not been submitted elsewhere for a degree.

Dr. K. Poddar

Professor

Department of Aerospace Engineering

Indian Institute of Technology

Kanpur 208016

August 2000

ACKNOWLEDGEMENTS

I would like to express my gratitude to my advisor Dr K Poddar, Professor, Department of Aerospace Engineering, I.I.T. Kanpur, for his constant supervision and guidance during the course of my M.Tech Program. Special thanks to Dr. E. Rathakrishnan, Professor, Department of Aerospace Engineering, I I.T. Kanpur for his affection towards me during my stay at I.I.T. Kanpur.

I am also thankful to Mr. K. Mohan and Mr. Rameshwar for their help in setting up the experiments. I express my appreciation and indebtedness to my friends Deepak, Sunil, Neelam and Gopal Sharma who apart from helping me in this work also made my stay at Kanpur very pleasant and memorable.

I can never thank enough my parents, brother Pushkar and sister Veenu. They have been a source of inspiration in my life and career, thus far.

Last but not least, I am grateful to the Almighty God who gave me courage to do the job efficiently.

Meenu Kapil

Department of Aerospace Engineering

Indian Institute of Technology

Kanpur 208016

August 2000

CONTENTS

LIST OF FIGURES

Nomenclature

Re	Reynolds number
U_∞	Freestream velocity
P	Static pressure measured w.r.t. free stream pressure
P_∞	Free stream pressure
ρ	Free stream density
Cp	Pressure coefficient
Cd	Drag coefficient due to pressure
D	Diameter of the main cylinder
R	Radius of the main cylinder
H	Height of the main cylinder
θ	Angular displacement of the main cylinder
ψ	Stagger angle
r	Distance of the pressure port on the disc from the center of the main cylinder
h	Distance of the pressure port on the surface of the main cylinder from the top

ABSTRACT

In the present investigation, a series of experiments have been conducted to study the phenomenon of flow interference between two identical infinite circular cylinders at different Reynolds numbers and for different arrangements. These experiments have been conducted in a low speed wind tunnel. The objective has been to form a preliminary idea of the effect that the upstream control cylinder has on the flow pattern around the main cylinder under different conditions. The variables in the present series of experiments are the stagger angles and the Reynolds numbers. With the stated objective in mind, the pressure distributions have been determined around the main cylinder at different stagger angles and Reynolds numbers and compared with those for the single cylinder in isolation at the same Reynolds numbers. The static pressure variation on the floor around the main cylinder has also been determined. A careful and detailed analysis of the experimental data has been carried out and important characteristics determining the flow like the points of flow separation have been identified. Plausible reasons for the observations have been included where possible. The drag coefficient on the main cylinder has been computed from the pressure distribution. The perpendicular distance between the two cylinders has been maintained constant at 6.5D, where D is the diameter of the two cylinders.

As expected, the effect of the control cylinder on the downstream cylinder is reduced as the stagger angle is increased i.e drag coefficient increases with the increase in stagger angle. This is indicated by the pressure distribution at $\psi = 20°$ which is the same as that on the single cylinder. Minimum drag is obtained in tandem arrangement or in other words the effect of control cylinder is greater in tandem arrangement than any other. Flow separation point moves farther in the downstream direction as the stagger angle decreases. There is no significant variation in the drag coefficients along the height of the cylinder. The Reynolds numbers in this series of experiments have a negligible effect on the values of the drag coefficient.

1. INTRODUCTION

The flow around bluff bodies is a far more complex phenomenon than the flow around streamlined bodies like airplanes. Circular cylinder belongs to a class of bodies, which may be termed as semi-aerodynamic when compared with streamlined bodies like airfoils and non-aerodynamic bodies like rectangular cylinders with sharp edges. Aerodynamic bodies avoid separation; Non-aerodynamic bodies have fixed flow separation points at some of the corners. In the case of semi-aerodynamic bodies, the points of flow separation vary with the freestream velocity, freestream turbulence, geometry and the surface roughness of the body.

The flow of an incompressible fluid at various Reynolds numbers around a single circular cylinder is one of the most challenging problems in bluff body aerodynamics considering both the theoretical and physical aspects. The problem assumes the twin reasons of its fundamental nature and its applications. Consequently it has been worked out in great detail, and admits of analytical, computational and empirical solutions. On the other hand, the problem of flow around a pair of circular cylinders in various arrangements is a step-ahead in terms of complexity and has been attacked mainly by way of wind tunnel experimentation and occasionally by computer simulations. This problem is also very important for the following reasons

(a) From fundamental stand point in that it constitutes one of the basic problems in the field of flow interference and
(b) In the light of its practical applications; a few of which are listed in the lines that follows
    1. Aeronautical Engineering: twin struts to support wings.
    2. Hydronautical Engineering: periscope, snorkel and radar mast vibrations.
    3. Civil Engineering: twin chimney stacks in winds and jetties and offshore structures in high seas.
    4. Electrical Engineering: twin conductor transmission line vibration.
    5. Mechanical Engineering: heat exchanger tube vibrations.
    6. Chemical Engineering: pipe rack forces etc.

The assumption that two cylinders should behave in a flow in a similar, or even an identical manner to a single cylinder is justified only when the two cylinders

are sufficiently apart. The interference between two cylinders at close proximity, however, drastically changes the flow pattern around them and produces unexpected forces and pressure distributions and intensifies or suppresses vortex shedding.

There are infinite numbers of possible arrangements of two parallel cylinders positioned at right angle to the approaching flow direction. Of the infinite arrangements two distinct groups may be identified: in one group, two cylinders are in a tandem arrangement, one behind the other at any longitudinal spacing; and in the second group the cylinders face the flow side by side at any transverse spacing. All other combinations of longitudinal and transverse spacing represent staggered arrangements. Of these, the staggered arrangement is relatively less worked upon and reported on. In the current investigation, the pressure measurements were carried out for two different Reynolds numbers and as many as five different staggered angles both on the tunnel floor and on the surface of the cylinder.

This static pressure distribution data is important in the light of the fact that it serves as an important tool in determining the velocity patterns around the main cylinder, in the absence of hot-wire measurements. There are two kinds of plots obtained from this floor data. In the first type of plots the variation in pressure at various circumferential angles with radial distances, r/R, is shown and the other is a set of pressure variation with circumferential angle at specific radial distances from the center of the cylinder of interest. It is very important to note that since the cylinders considered are infinite in extent, the static pressure distribution determined at the floor of the tunnel carries over to horizontal planes at various heights along the cylinder's height.

1.1 LITERATURE REVIEW

At Reynolds numbers above 10000 the flow around a circular cylinder can be separated into at least four different regimes: sub-critical, critical, supercritical and transcritical (Roshko) [1]. The lowest regime, the subcritical, continues to a Reynolds number, Re, of about 200000. In this regime the boundary layers separate in a laminar state at about 80° from the forward stagnation point, and the early separation induces a high drag coefficient of about 1.2 with an associated Strouhal number of about 0.2.

Many studies have been directed towards the case of steady flow past groups of cylinders. Zdravkovich [2], [3] has reviewed the problem of mutual interference between pairs of circular cylinders in a steady flow. He made particular reference to the side-by-side and in-line arrangements of the cylinder pair.

Pannell, Griffiths, and Coales [4] measured the force on two parallel circular wires. The distance between the centers of the two wires varied between 1 dia to 6 dia. They measured combined drag force in tandem arrangement and also in the staggered position at various stagger angles up to 20°. The angle of stagger is the angle joining the centers of the two wires and the airflow direction. For this measurement the Reynolds number was 9.72×10^3. They found that the minimum drag for the two wires in contact was only 40% of the drag on one wire alone. This was due to an improved streamlining of the flow pattern for the latter case.

In 1933, Bierman and Herrnstein [5] measured the force on a pair of circular cylinder in the Reynolds number range 5.5×10^4 to 1.4×10^5. The drag force was measured separately for each cylinder. They introduced an interference drag coefficient C_{Di} defined as the difference between the drag coefficients measured on one of the cylinders in tandem and the drag coefficient of the single cylinder at the same Re. The interference drag coefficient of the upstream cylinder was found to be almost zero when the cylinders were in contact. As the spacing increased, C_{Di} decreased and reached a minimum value at the spacing ratio of 3.5. Beyond that spacing, it rapidly increased and became zero again 5 diameters onwards. The interference drag of the downstream cylinder was found to be negative when the cylinders were in contact. A rapid increase followed the increase of spacing. An interruption of the rate of increase occurred at the spacing where the C_{Di} of the

upstream cylinder was a minimum. This odd kink did not attract the attraction of the later investigators.

This presence of the kink on the drag curve was verified at the University of Salford by Zravkovich and Pridden [6]. Both the cylinders were placed between two parallel panels in order to exclude the end effects. The kink might be due to some change in the flow pattern either in the gap between the cylinders or in the wake behind the downstream cylinder. To investigate further, a third cylinder was placed in tandem. The second cylinder was monitored and both the gap in the front and at the rear were kept the same. The kink did not disappear. So it is concluded that the kink is caused by some change in the flow pattern in the gap.

In 1972 the base pressure and vortex shedding behind the cylinders was measured by Ishigai et al. [7]. They found a jump both in the Strouhal number and in the base pressure at the critical spacing of 3.8 D. The Reynolds number was kept at 8 x 10^3.

Hori [8] was the first who conducted the experiment for the pressure distribution around the two cylinders in tandem and staggered arrangements. He rotated the cylinder pairs and exposed them in staggered arrangements to the wind for three spacings (1.2, 2.0, and 3.0). The pressure distribution around the upstream cylinder showed that only the rear part of it was affected by the presence of the downstream cylinder. The base pressure coefficient increased as the spacing of the downstream cylinders increased and consequently the drag force of the upstream cylinder was reduced. Hence, the drop of the base pressure caused the decrease of the interference drag only. The pressure distribution around the downstream cylinder showed two unusual features. The first was that the side facing the gap between the cylinders had a very low negative pressure which was almost the same as the corresponding value of the base pressure of the upstream cylinder. This fact implies that the flow in the gap is almost stagnant. Secondly, the negative gap pressure coefficient in front of the downstream cylinder exceeded that on the base side behind. Hence the downstream cylinder experienced a negative drag force. The decrease of the interference drag was caused mainly by the corresponding increase in the gap pressure.

Zdravkovich and Stanhope [9] carried out pressure measurement around the downstream cylinder at higher Reynolds numbers. They have performed the experiment for six different spacings from 1.5 D to 7 D. They found that there was a sudden change in the flow pattern in the gap when the spacing was increased beyond 3.5 D. Apart from this there has been other investigations relating to pair of circular cylinders [10-20].

1.2 PRESENT INVESTIGATION

The present work is an experimental investigation of the phenomenon of flow interference between two circular cylinders for different arrangements and Reynolds numbers. The effect of the presence of an infinite upstream cylinder on the flow around an identical downstream cylinder has been determined. This has been done by carefully recording the pressure distribution around the downstream cylinder for different Reynolds numbers and by comparing this distribution with that around the single cylinder at the same Reynolds numbers. The static pressure distribution has been determined on a plane at the base of the cylinder (i.e. at the tunnel floor) under consideration and its variation has also been studied. The pressure distribution has been determined at fourteen equidistant planes parallel to the base along the height of the cylinder. The L/D ratio is maintained constant at 6.5 where L is the distance between the two cylinders in the tandem arrangement and D is the diameter of the main or downstream cylinder. The variable parameters in this study are the Reynolds numbers and stagger angles. The Reynolds numbers were 13200 and 19800. For each of these Reynolds numbers the downstream cylinder was placed at stagger angles of $0°$, $\pm 10°$ and $\pm 20°$ with respect to the upstream cylinder.

2. EXPERIMENTAL SET-UP

In this chapter a complete description of experimental facility with experimental model and brief account of the fabrication process involved has been explained. The procedure for conducting the experiment and instrumentation has also been explained.

2.1 THE WIND TUNNEL

Experiments were carried out in an open circuit suction type wind tunnel, which is installed in a closed room. Air is sucked into a settling chamber of 1300 mm x 1000 mm cross-section having honeycomb at its inlet followed by four wire mesh screens. Following the settling chamber, there is one 2-D contraction with an overall contraction ratio of 9. The test section is followed by a diffuser at the end of which is mounted an axial fan and motor assembly. The 2 H.P. D.C. motor of variable speed type is used. The maximum attainable speed at the inlet of the test section is about 10 m/s.

The rectangular test section of the wind tunnel has a cross-section of 400 mm x 300 mm, and a length of 900 mm. One of the sidewalls and the floor is made of wood and sun-mica. The other sidewall and the roof are made of perspex. A span-wise groove of 15 mm width is cut out at an upstream distance of 310 mm from the center of the main cylinder.

2.2 MODEL GEOMETRY

The model essentially consists of two cylinders – the main cylinder and the control cylinder. The total pressure distribution around the main cylinder is the physical quantity of direct interest in this series of experiments. This distribution is determined and subsequently analyzed both in the absence of an upstream flow control cylinder and in its presence at various stagger angles. A brief description of the main cylinder, the flow control cylinder, and the relative positions of the two cylinders during the course of the experiments follow.

2.2.1 THE MAIN CYLINDER

This cylinder is a hollow brass model with an outer diameter of 50 mm. It is centrally mounted on a perspex disc of diameter 310 mm as is shown in figure (1).

This cylinder is of infinite height, that is, its height is the same as that of the wind tunnel test section. This is to ensure two dimensional flow conditions. There are fourteen pressure ports each on diametrically opposite sides of the disc and twelve ports each on either side of the disk. These ports are all of 1 mm diameter. It is to be noted that a cutting plane passing through the centers of all ports on the disc also split all the ports on the cylinder centrally into two equal halves each. The disc sits inside a specially prepared groove in the tunnel floor.

2.2.2 THE CONTROL CYLINDER

The flow control cylinder is basically a hollow steel cylinder with outer diameter of 50 mm. This cylinder is placed upstream to the main cylinder at various stagger angles. It has no pressure ports or any other instrumentation. It is a bluff body placed to create a disturbance in the flow upstream to the main cylinder. Essentially therefore the main cylinder is placed in the wake of this cylinder. The objective is to study the alterations in the flow around the main cylinder due to the presence of this control cylinder at various stagger angles, as determined to an extent by aerodynamic parameters such as the pressure coefficients, which are determined for the main cylinder. Like the main cylinder, the upstream flow control cylinder is also of infinite height.

2.2.3 RELATIVE POSITIONS OF THE TWO CYLINDERS

The control cylinder is placed at a distance of 6.5 D from the center of the main cylinder, D being the diameter of the main cylinder. It is placed upstream to the main cylinder as shown in figure (2). It is moved along a line perpendicular to the flow direction at this same distance or stagger angles 0°, ±10°, and ±20° respectively, for different air speeds.

2.2.4 PRESSURE MEASUREMENT AROUND THE MAIN CYLINDER

The disc with the main cylinder mounted sits inside a specially prepared groove in the tunnel floor. A linear mark is made on the tunnel floor inline with the flow direction. Initially the disc is so positioned that the disc port line is aligned with this mark. In this configuration, the flow is parallel to the cutting plane. Measurements were made first for this configuration. The disc is subsequently rotated by 10° to the flow so that the ports facing the upstream direction initially were now

stationed at 10° to the flow direction and the ones downstream were stationed at 190°. Differential pressure readings were now taken. Nineteen such cycles of measurements and rotations at 10° angles resulted in determining the pressure distribution around the main cylinder.

2.3 INSTRUMENTATION

All in all there were 52 points at which the differential pressure was to be measured. The basic unit used is one supplied by M/s Furness Control. It consists of one master unit and two slave units each having 20 channels. This unit is interfaced to a Pentium II computer via a data acquisition board PCI 6024E, supplied by National Instruments. The software used for data acquisition and analysis is LabVIEW, a National Instruments product for Computer Based Instrumentation, or more popularly, Virtual Instrumentation. Front panels and block diagrams of the instruments designed during various stages of the work have been included along with a statement of their specific purpose.

Experiments were carried out at different Reynolds numbers (13200 to 26667) based on the diameter of the main cylinder. A pitot-static tube was used to measure the total and static pressures. The pitot-static tube was connected to a digital micro-manometer (model-FC012 manufactured by Furness Controls Ltd., Bexhill, England), which gave the velocity in mm as well as in m/s.

3.RESULTS AND DISCUSSIONS

This chapter includes the results of the experiment conducted. In presenting the data the following co-ordinate system has been adopted. The origin of the co-ordinate system is taken as the center of the circular cylinder at mid-span of the test section. The flow direction is taken as x-axis. z-axis is taken along the vertical height of the model. The axis perpendicular to the x-axis and the model vertical axis is taken as y-axis. This co-ordinate system is shown schematically in figure (1).

3.1 PRESSURE DISTRIBUTION ON THE MAIN CYLINDER SURFACE (WITHOUT CONTROL CYLINDER)

Figures (3a) to (3c) show the local pressure distribution on the single cylinder at three different Reynolds numbers of sub-critical range. These three Reynolds numbers are 13200, 19800 and 26667. The distribution of the pressure was measured in the steps of $\theta = 10°$ around the circumference of the cylinder. In these figures the pressure distribution is plotted against the circumferential angle θ of the cylinder.

Figure (3a) shows the case of sub-critical flow at Re = 13200. It is observed that the pressure distribution is positive from $\theta = 10°$ to $\theta = 25°$ and $\theta = 330°$ to $\theta = 360°$. The coefficient of pressure is minimum at $\theta = 60°$ and $\theta = 290°$. According to the Bernoulli's theorem at these points velocity of the flow is maximum. As seen from the figure the pressure distribution is symmetrical for the upper and lower halves of the cylinder. Hence, there is no lift. But the pressure coefficient Cp over the rear portion of the cylinder remains negative. This destroys the symmetry about the vertical axis and produces a drag force in the direction of the flow. As indicated by the graph the boundary layer separates at about $\theta = 80°$ and $\theta = 280°$ before reaching the main cross-section. In this case the drag force is calculated in terms of the drag coefficient, Cd_p and is found to be 1.2. The drag coefficient, Cd_p is calculated by integrating the pressure distribution,

$$Cd_p = \frac{1}{2}\int_0^{2\pi} Cp\cos\theta$$

Figure (4) shows the relation between drag coefficient and Reynolds number for circular cylinder. This graph [21] is for the validation of Cd. It can be seen from

this figure that Cd is 1.2 for Re =13200 which is same as calculated in the previous case.

Figure (3b) and (3c) show the behavior at Re = 19800 and Re = 26667. Also for both the Reynolds numbers the boundary layer separation occurs at $\theta = 80°$ and $\theta = 280°$. In these cases the drag is also found to be 1.2. Because these three Reynolds numbers i.e. 13200, 19800 and 26667 fall in the middle sub-critical zone and in this zone the drag coefficient remains same for Re = 10000 to Re = 100000.

3.2 PRESSURE DISTRIBUTION ON THE MAIN CYLINDER SURFACE (WITH CONTROL CYLINDER)

In this case the control cylinder was placed at a distance of 6.5D from the center of the main cylinder, where D was the diameter of the downstream cylinder. It was moved along the line perpendicular to the flow direction for different stagger angles. Stagger angle is the angle between the line joining the centers of the cylinders and the flow direction. The downstream cylinder i.e. the cylinder around which the pressure distribution is determined lies in the wake of the control cylinder. The control cylinder is placed at some stagger angle.

3.2.1 TANDEM ARRANGEMENT

This is the case where the stagger angle is zero, i.e., the cylinders are in line with each other and parallel to the flow direction. Figure (5a) shows the pressure variation with θ at stagger angle of 0° and Reynolds number of 13200. As can be seen from the figure the Cp value decreases from 0.6 at angle of 0° to a local minimum of –1.1 at an angle of 70°. It then rises uniformly to a value of –0.8 at angle of 120° where flow separation takes place. Flow separation also takes place at symmetrically opposite end corresponding to $\theta = 240°$. It falls to a local minimum of –0.8 at $\theta = 290°$ and subsequently rises smoothly to a value of 0.6 at $\theta = 360°$. The above mentioned experimental observation can be accounted for as follows. First of all it is to be noted that gap pressure coefficient drops to 0.6 at $\theta = 0°$ in the case of tandem arrangement whereas it assumes a value of 1.0 in the case of single cylinder. This is because in the case of tandem arrangement the point on the downstream cylinder corresponding to $\theta = 0°$ lies in the wake of upstream cylinder. The flow velocities are higher in this region. This results in lower values of gap pressure and the Cp value

measured at $\theta = 0°$ of the downstream cylinder is correspondingly lower. These values are lower than the corresponding values for the single cylinder since the effect of the control cylinder is reduced. At $\theta = 180°$ there is a slight increase in Cp. This is also reported in Hori [8].

3.2.2 STAGGERED ARRANGEMENT

Figure (5b) shows the variation of pressure with θ for the positive stagger angle of 10° and Reynolds number is 13200. It can be seen from the graph that for values of circumferential angles $\theta < 20°$ and $\theta > 322°$, Cp assumes positive values. Between $\theta = 20°$ and $\theta = 322°$ pressure distribution is negative. It is clear from the graph that for the upper half the value of Cp is minimum at around 60°. Likewise for the lower half, Cp takes near minimum value at $\theta = 290°$. It is observed that there is a slight difference between the two minimums with the minimum in upper half being slightly higher than that at the lower half. This can be accounted for as follows. The flow in the wake of the control cylinder is turbulent. The upper half of the downstream cylinder lies in wake of the upstream or control cylinder and therefore the flow velocities in the upper half are higher than those in the lower half. Clearly, therefore, the corresponding Cp values are lesser in the upper half than those in the lower half.

It is seen that the minimum Cp value in the case with the control cylinder is higher than the one without. This can be accounted for as follows. There is net momentum transfer between the shear layers from the turbulent region in the upper half of the cylinder to the lower layers. This is because of the fact that air being a real fluid has a finite measurable viscosity. This momentum transfer affects an increase in the velocities of fluid in the lower half and thereby the lower pressure coefficient.

Figure (5c) shows the case of negative stagger angle of 10° at same Reynolds number as in previous case i.e. at 13200. In this case the situation is reversed i.e. the values originally determined for the upper and the lower halves (with positive stagger angle of 10°) are interchanged within limits of experimental accuracy. In other words, figure (5c) is the mirror image of the figure (5b). At stagger angle $\Psi = 20°$ and Re = 13200 [figure (5d)] the graph obtained is more or less similar to the without control

cylinder and this implies that the control cylinder does not cause aerodynamic interference with the main cylinder anymore.

For Re = 19800 and stagger angles 10°, -10°, -20° the corresponding plots can be seen in figure (6a), (6b), and (6c) respectively. It is to be noted that these plots are similar to the ones for Reynolds number 13200 and the respective stagger angles. This observation can be accounted for by the fact that the two Reynolds numbers are of the same order of magnitude and fall in the same range.

3.3 ANALYSIS OF FLOOR DATA:

The static pressure distribution was determined on the floor around the main cylinder under various conditions and the Cp values calculated. Figures (7a) to (7c) include the plots of variation of Cp with the radial distances measured from the origin of the main cylinder. The analysis of this data follows for the following representative cases.

1. Re = 26667, without control cylinder
2. Re = 19800, tandem arrangement ($\psi = 0°$)
3. Re = 13200, stagger arrangement ($\psi = 10°$)

The plots for the cases with stagger angles of ±20° are similar to the plots in the single cylinder cases and do not need to be discussed separately. This observation can be explained by noting that when the downstream cylinder is placed at stagger angles of ±20°, it is not much affected by the presence of the control cylinder. A similar observation is made while analyzing the Cp versus θ graphs for the cylinder surface.

The upper plot in each of these figures shows the Cp Versus r/R curves for the upper half of the cylinder with θ varying between 0° and 180° while the lower one shows the same curves for θ between 180° and 360°. In the case of single cylinder and tandem arrangements, therefore, the two plots in each of these figures are the same and also do not merit separate discussions.

Also, for negative stagger angles, the two plots in each of the figures for the corresponding positive stagger angles are simply interchanged. This is because the relative positions of the upper and lower halves of the downstream cylinder with respect to the upstream cylinder are swapped. And this observation is also clear from

the Cp-θ plots for cylinder surface for the corresponding positive and negative stagger angles in which case the plots are mirror reflections of each other. Therefore, it is sufficient if the discussion is restricted to the positive stagger angles alone. Reynolds number dependent phenomenon across the plots is analyzed separately.

3.3.1 PRESSURE VARIATION WITH RADIAL DISTANCE FOR Re = 26667 (WITHOUT CONTROL CYLINDER)

For θ = 0°, 10° and 20°, it can be seen from figure (7a) that the Cp values are higher at the ports closer to the cylinder than at the ones away from it. This is explained by noting that the static pressures are highest at points nearer the cylinder because the flow encounters an obstacle and is retarded to smaller velocities in this region.

Beyond the sixth port or so, the Cp values are very nearly the same and are close to the freestream pressure. At these ports the effect of the cylinder and the flow pattern is negligible enough for all practical purposes.

For θ = 40° through θ = 80° the static pressures at the first port are lower than the static pressures at the second port clearly indicating that the flow velocity in the immediate vicinity of the cylinder is higher than in a region just beyond it. Thereafter, they rise very gradually and stay nearly constant after about the fifth port where they become close to the freestream pressures, indicating the declining effect of the cylinder at these ports.

From the Cp-θ curve (for the cylinder) for this case it is clear that separation at this Reynolds number takes place at an angle of 80°. For 90° and 100° angles the static pressure curves rise more steeply indicating that the initial ports lie in the wake where the velocities are high and the pressures low. An inclined 'S' shaped curve is seen for the curves closer to θ = 180°. Most of the ports on these lines lie inside the wake. The pressures are seen to fall initially to a minimum at around the third port. Subsequently there is a slightly steep rise in the pressures which continues till about eighth port. Then there is 'plateau' portion where the pressure rises gradually and eventually equals the freestream pressures. The pressure drops to the minimum of the third port. This can be explained by the phenomenon of flow reversal or back flow which increases the flow velocity to a maximum at around the third port. Pressure

decreases at the second and the first ports as the reversed flow now gets retarded in the direction of the cylinder.

3.3.2 PRESSURE VARIATION WITH RADIAL DISTANCE FOR Re = 19800 (TANDEM ARRANGEMENT)

From Cp-θ plots for the cylinder, it is clear that the separation is delayed in the case of the tandem arrangement when compared to the case of the single cylinder. This results in a narrower wake behind the downstream cylinder and consequently a reduced drag. The Cp vs r/R plots in the case of the tandem arrangement at Re = 19800 can be seen in figure (7b). The downstream cylinder lies completely in the wake of the control cylinder. Cp values are seen to be highest at first port for the 0°, 10° and 20° lines and can be seen to decrease gradually. After about the fifth or sixth port they can be seen to assume negative values. The static pressures are significantly lower at the ports on these curves when compared with the curves for the case of the single cylinder. This is because of the increased flow velocities. The negative values can be accounted for by the increased Reynolds number flow in the wake.

The curves for angles between 30° and 120° can be seen to start at relatively lower values of Cp and gradually rise to increasing values of Cp at subsequent ports. Cp values in the wake of the downstream cylinder are found to be significantly lower than those at upstream ports. This is because the turbulence and Reynolds numbers are still higher in this region. Vortex formation and back flow explain the drop in the Cp value at the second port for the 180° curve in this case, too.

3.3.3 PRESSURE VARIATION WITH RADIAL DISTANCE FOR Re = 13200(STAGGERED ARRANGEMENT, ψ = 10°)

The staggered arrangement presents an interesting case study because the static pressure distribution around the upper and lower halves of the downstream cylinder are asymmetric, which implies that the upper and lower plots for these cases are different and need to be explained separately. Figure (7c) shows the plots for the case Re = 13200 and ψ = 10°.

Case 1: The upper half or the case from θ = 0° to 180°

The Cp values at the first port range between –1 and 0.55. These values are comparable with and even greater than the corresponding static pressure values for the

case of the single cylinder. However, they are higher than the values obtained for the tandem arrangement. The latter observation is easily explained by noting that the flow velocities and Reynolds numbers are higher because the downstream cylinder lies completely in the turbulent wake of the control cylinder in the case of the tandem arrangement. The former observation is counter-intuitive because it implies that the flow velocities are lower in the staggered arrangement when compared to the single cylinder at the same Reynolds number. This is probably because of the flow pattern that emerges the very complicated interaction between the turbulent wake of the upstream cylinder and the laminar layers near the downstream cylinder. This can be partially attributed to pressure recovery. The $\theta = 0°$, $10°$, $20°$ and $30°$ curves follow a similar trend with the static pressures at the latter ports and declining to a nearly steady value around the seventh port or so. From $\theta = 40°$ through $\theta = 90°$, the curves follow a trend similar to the case of the single cylinder except that the static pressures are higher from 90° through 180°, also curves follow a similar trend to the case of the single cylinder with the only difference that static pressures are higher.

Case2: Lower half or the case from $\theta° = 180$ to $\theta = 360°$

Static pressure declines to a nearly steady value at about sixth port or so. The decline is rapid in comparison with the single cylinder. The curves are similar to the case of the single cylinder with the difference as the above that the pressure values are relatively less.

3.4 STATIC PRESSURE VARIATION WITH THETA AT DIFFERENT RADIAL DISTANCES

The C_p - θ plots at specific radial distances from the center of the cylinder around which pressure measurements have been made are included in figures (8a) through (8c). These graphs assume significance because they give a clearer picture of the static pressure distribution around the cylinder of concern. Three typical plots have been discussed in this report since the explanations of the remaining plots follow along similar lines. These plots are:

1. Pressure variation with radial distance for Re = 26667
   (without control cylinder)
2. Pressure variation with radial distance for Re = 13200
   (Tandem Arrangement)

3. Pressure variation with radial distance for Re = 19800 and ψ = 10° (Staggered Arrangement)

Reynolds number dependent phenomena, across the plots, have been explained separately.

3.4.1 PRESSURE VARIATION WITH THETA FOR Re = 26667 (WITHOUT CONTROL CYLINDER)

First of all, it is observed that the plots are symmetric about the line θ =180° which implies that the static pressure distribution is the same on the upper and the lower halves of the single cylinder. It can be seen from figure (8a) that the Cp values at the first port start out at roughly 0.45 and decline steeply to a value of around –1.35 at θ = 170°. It then falls to a minimum of about –1.45 at around θ = 190° and rises again, in a way more or less similar to the trend it followed during the descent. Further, it can be clearly made out from the figure that the static pressure decreases with an increase in the radial distance of the ports i.e., the static pressures measured at successive ports indicate a declining trend. This is easily explained by the fact that the fluid velocities are lower in the vicinity of an obstacle, in this case, the cylinder. A very interesting observation in the case of these plots is that the Cp values at all ports are clustered in the range θ = 40° through θ = 60°. This is also true between θ = 300° and θ = 320°, i.e., the Cp values are clustering in the neighborhood of θ = 50° and θ = 310° lines. The Cp values at all ports along these lines are more or less the same and are very close to zero. This indicates that the pressures along these lines are more or less close to the freestream pressure. The flow is clearly not much affected by the presence of the cylinder at these ports. It retains its laminar characteristics in this region. In all likelihood, the flow easily bends over and thereby experiences the least resistance to its motion in this region. The earlier plots of the floor data indicate that the pressures are the least at around the second or the third ports at θ = 180°, i.e., the velocities are the highest in this region. This important observation is also borne out by the current plot (8a). A very important common characteristic of all these curves is that they start out at some value of Cp, show a relatively smooth decline till about θ = 160° and then dip very quickly to lowest values of Cp at around θ = 180°. This observation indicates that the flow retards very quickly in the near vicinity of the cylinder, than at points relatively away from it.

3.4.2 PRESSURE VARIATION WITH THETA FOR Re = 13200 (TANDEM ARRANGEMENT)

The plots constituting figure (8b) are relatively flat in comparison with those of the single cylinder. While they retain the overall characteristics of the plots in the case of the single cylinder in that they are also symmetric about the line $\theta = 180°$ and in the shape of the curves, there are certain differences that must be taken note of. In the first place, the Cp values start out at relatively lower values, which mean lower static pressures at these ports and correspondingly higher flow velocities in the region around the cylinder of interest. It must be noted that the Cp values decline, but not so markedly, and to relatively higher values than in the case of the single cylinder before they begin to rise again. Here again the clustering takes place in nearly the same region with the only difference that they appear to be spaced closer. This implies that the control cylinder contributes little in altering the location of the region in which the static pressures are acquiring velocities closer to the freestream pressure. Moreover in this case there is no sharp decline in the static pressure values around $\theta = 180°$ and the minimum values are rather flat and less well defined. This implies that there is an entire region where the static pressures assume the lowest set of values instead of a sharply defined location. In this region, the flow velocities are the highest.

3.4.3 PRESSURE VARIATION WITH THETA FOR Re = 19800 AND $\psi = 10°$ (STAGGERED ARRANGEMENT)

In the figure (8c) the staggered arrangement presents a very interesting case study since the pressure distribution is not symmetric in this case about the line $\theta = 180°$. Therefore, we can study the pressure distributions around the upper and the lower halves of the cylinder separately.

Upper Half

The static pressures in the successive ports for the staggered arrangement are in general, higher than the corresponding static pressures in the case of tandem arrangements and lower than the single cylinder. Clustering takes place around the same region as in the cases discussed previously in the upper half of the cylinder. In this case however, clustering occurs at a value slightly less than the freestream value. The minimum values are relatively less well defined in this case than in the case of the single cylinder but more well defined than in the tandem arrangements of the two

cylinders. The decline in the pressure values is steeper than the tandem arrangement but lesser than the decline in the case of the single cylinder. The minimum values are seen around $\theta = 160°$ and $170°$

Lower Half

The lower half of the cylinder shows an increase in the Cp values, indicating that velocities are now decreasing away from the immediate wake of the cylinder. Clustering takes place at around $\theta = 320°$, and this time around values, closer to the freestream pressures unlike the upper half. For all practical purposes, the rest of the characteristics of these curves are similar to the upper half of the main cylinder and there are no noteworthy characteristics.

3.5 VARIATION OF DRAG COEFFICIENT WITH HEIGHT

Figure (9) shows the profile drag coefficient variations at different heights along the axis of the cylinder. The profile drag coefficients were computed by integrating $Cp\cos\theta$ numerically between 0 and 2π. Coefficient of drag is least for tandem followed by 10°, 20° and the single cylinder. The drag coefficients under various conditions are plotted at different heights. It can be seen that there is no significant variation in the profile drags.

3.6 VARIATION OF DRAG COEFFICIENT WITH STAGGER ANGLE

For different stagger angles, the drag coefficients are plotted in figure (10). The drag coefficient is found to be the lowest in the case of tandem arrangement and

3.7 SURFACE PLOTS AND CONTOUR PLOTS FOR CYLINDER:

Variation of pressure with circumferential angle, θ, at different heights is shown in figures (11a) through (11c). They are essentially representative of the pressure variation with the circumferential angle θ, at various heights along the axis of the cylinder. Sections of the surface plots have been analyzed in the previous sections and therefore these surface plots do not merit separate discussion. Figures (12a) through (12d) show the contours of the pressure coefficients for the main cylinder at different arrangements and figures (12e) through (12h) show the contours of the pressure coefficients for the floor at different arrangements.

4. CONCLUSIONS AND DISCUSSION

The boundary layer separation takes place at relatively small (80° and 280°) circumferential angles in the case of the single cylinder at all Reynolds numbers. The drag coefficient in all these cases for the single cylinder has been found to be 1.2. The boundary layer separation is delayed in the case of the tandem arrangement for the Reynolds numbers considered. The coefficient of drag (0.72) calculated for this arrangement is also the least indicating that the downstream cylinder experiences least aerodynamic resistance in this arrangement. The coefficient of drag is computed to be 0.88 in the case of the cylinders placed at a stagger angle of 10°. The coefficient of drag is computed to be 1.1 in the case of the cylinders placed at a stagger angle of 20°. This leads to the conclusion that increasing interference leads to lower drags for the Reynolds numbers considered. The effect of the upstream control cylinder on the flow pattern around the main downstream cylinder reduces as the stagger angle increases. This is clear from the fact that the pressure distribution around the main downstream cylinder for stagger angle of 20° is more or less the same as that of the single cylinder. The Reynolds numbers in this experiment have a negligible effect on the values of the drag coefficient. In general, the base pressures are found to increase as the stagger angle is increased. On the contrary, the gap pressures are found to decrease with an increase in the stagger angle. The upstream static pressures are found to gradually decrease and assume freestream pressure values whereas in the downstream portion the static pressures are found to gradually increase and assume freestream pressure values as the radial distance from the center of the main cylinder increases. As a manifestation of the phenomenon of vortex formation and back flow, pressure values are found to drop to a minimum at a certain distance in the wake of the cylinder. For the case of the 10° stagger angle, the C_p values are comparable with and even greater than the corresponding static pressure values around the first port for the case of the single cylinder and are higher than the values obtained for the tandem arrangement. Again, in this case, the decline in the static pressure values with the radial distance is rapid in comparison with that in the case of the single cylinder. The control cylinder contributes little in altering the location of the region in which the static pressures are acquiring velocities closer to the freestream pressure. Finally, there is no significant variation in the profile drags along the height of the cylinder.

4.1 SCOPE FOR FUTURE WORK

Hot-wire measurements can be performed to determine the velocity profile around the main cylinder. Flow visualization may also be done. The spacing between the two cylinders may be varied. Computer simulation of the flow field employing turbulent flow models may be done. The same experiments may be repeated for a wide range of Reynolds numbers. Flow around finite cylinders may be studied in similar arrangements. The side-by-side arrangement of the two cylinders may also be considered.

REFERENCES

1. Roshko, A. (1961), "Experiments on the Flow Past a Circular Cylinder," *J. Fluid Mech.* Vol. 10, pp. 345.
2. Zdravkovich M.M. (1977a), "Review of Flow Interference Between Two Circular Cylinders in Various Arrangements," *J. Fluids Eng. ASME*, pp. 618-633.
3. Zdravkovich M.M. and Pridden D.L. (1977b), "Interference Between Two Circular Cylinders; Series of Unexpected Discontinuities," *J. Ind. Aerod.*, Vol.2, pp. 255-270.
4. Pannell J.R., Griffiths E.A. and Coales. J.D. (1915), "Experiments on the interference between pairs of aeroplanes wires of circular cross-section," *Aero. Res. Council*, Rep, Memo, 208.
5. Biermann D.and Herrnstein W.H., Jr., (1933), "The Interference Between Struts in Various Combinations," *National Advisory Committiee for Aeronautics*, Tech. Report. 468.
6. Zdravkovich M.M and Pridden D.J. (1975), "Flow Around two circular cylinders; Research Report," *Proc. 2nd US National Conference on Wind Engineering Research*, Fort Collins, IV: 18
7. Ishigai S., Nishikawa E., Nishimura K.and Cho K. (1972), "Experimental Study of Structures of Gas Flow in Tube Banks with Tube Axis Normal to the Flow. Part 1: karman Vortex Flow Around Two Tubes at Various Spacings," *Bulletin of Japan Soc. Mech. Eng.*, Vol. 15, pp. 949-956.
8. Hori E. (1958), "Experiments on Flow Around a Pair of Circular Cylinders," *Proc. 9th Japan National Congress for Applied Mechanics*. Tokyo, pp. 231-234.
9. Zdravkovich M.M., and Stanhope D.J., (1972), "Flow Pattern in the Gap Between Two Cylinders in Tandem," *University of Salford Internal Report FM 5/72.*
10. Zdravkovich M.M., Feb (1972), "Smoke Observations of Wakes of Tandem Cylinders at Low Reynolds number," *The Aeronautical Journal*, Vol.76, pp.108-114.

11. P.W. Bearmann and A.J. Wadcock, (1973), "The Interaction Between a Pair of Circular Cylinders Normal to Stream," *J.Fluid Mech.*, Vol. 61, pp. 499-511.

12. Mair, W.A. and Maull D.J., (1971), "Aerodynamic Behavior of Bodies in the Wake of Other Bodies," *Transactions Royal Society*, A, Vol. 269, pp. 425-437.

13. Roshko A. (1955), "On the Wake and Drag of Bluff Bodies," *J. Aeronautical sciences*, Vol. 22, pp. 124-132.

14. Cooper, K.R. (1974), "Wind Tunnel Measurements of the Steady Aerodynamic Forces on a Smooth Circular cylinder Immersed in the Wake of an Identical cylinder," *National Aerodynamic Establishment Canada*, LTR-LA-119.

15. Shiraishi, N., Matsumoto, M. and Shirato H. (1986), "On Aerodynamic Instabilities of Tandem Structures," *J. Wind Eng. And Ind.Aerod.*, Vol. 23, pp. 437-447.

16. Yokoyama K., Sato H. and Kanzaki K., (1985), "On Aerodynamic Properties of Twin Cables in Proximity Arrangements," *Proc. Of the 40th Nat. Congress of JSCE*. No.I-217.

17. Dryden H.L., Hill G.C. (1930), "Wind Pressure on Circular cylinders and Chimneys," *Bureau of Standards Journal of Research,* Vol. 5, pp. 653-693.

18. Taylor G.J. (1915/16), "Pressure Distribution Round a Cylinder," *Technical Rep. Adv.Com. for Aeronamities*,

19. Cooper K.R. and Wardlaw R.L. (1971), "Aerodynamic Instabilities in Wakes," *Proc. of the International Conf. on Wind Effects on Build. And Struc.* pp. 647-655.

20. Zdravkovich M.M. "Flow Induced Vibrations of Two Cylinders in Tandem and their Suppression," Flow Induced Stuctural Vıbrations, *Karlruhe 1972, Springer Verlag 1974*, pp. 631-639.

21. Ito. M. (1990), " Bluff Body Aerodynamics and its Applications," A Selection of Papers Presented at *The Int. Colloquium on Bluff Body Aerodynamics and its applications*, oct.1988, Kyoto, Japan.

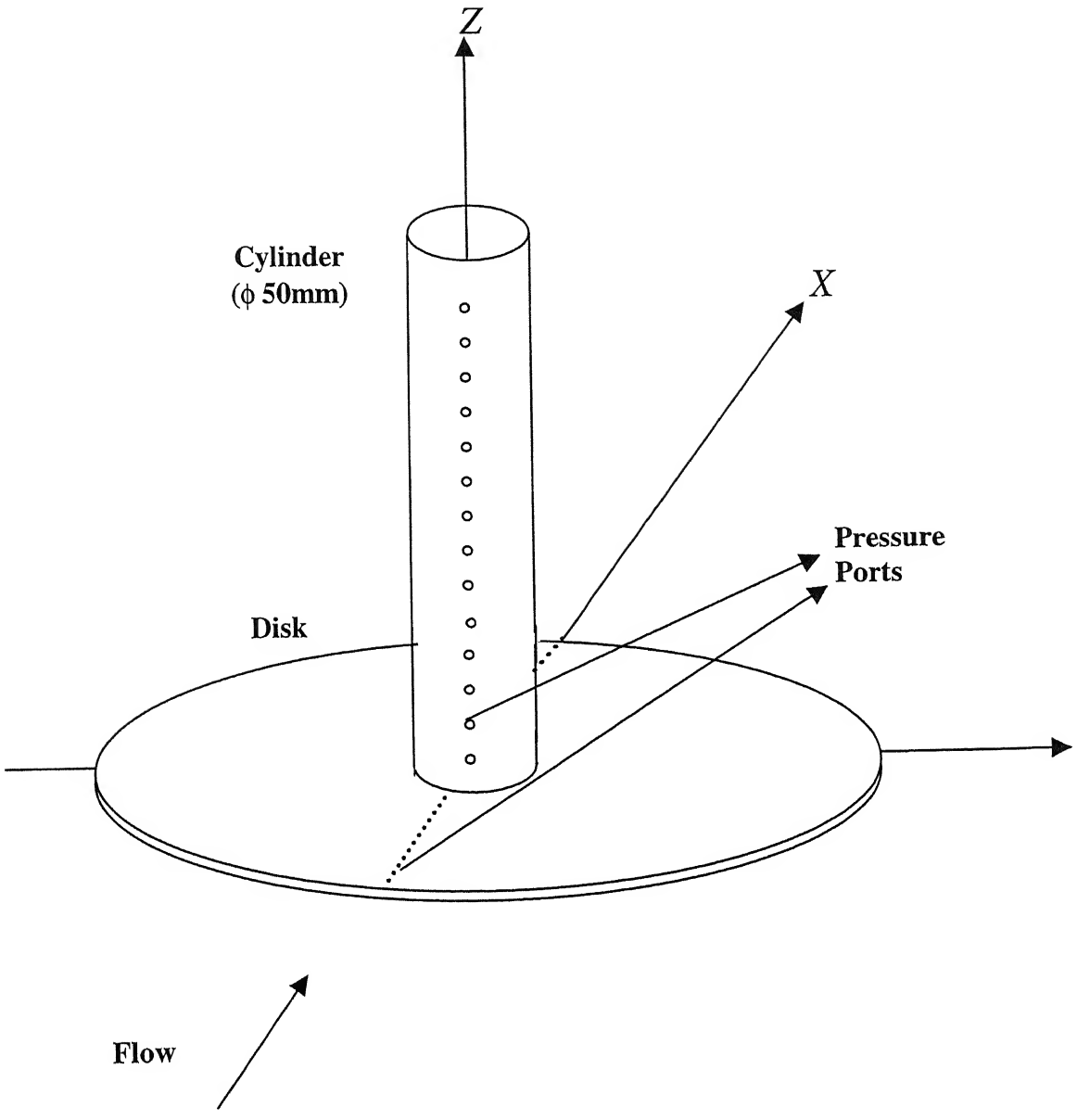

Figure 1. Main Cylinder

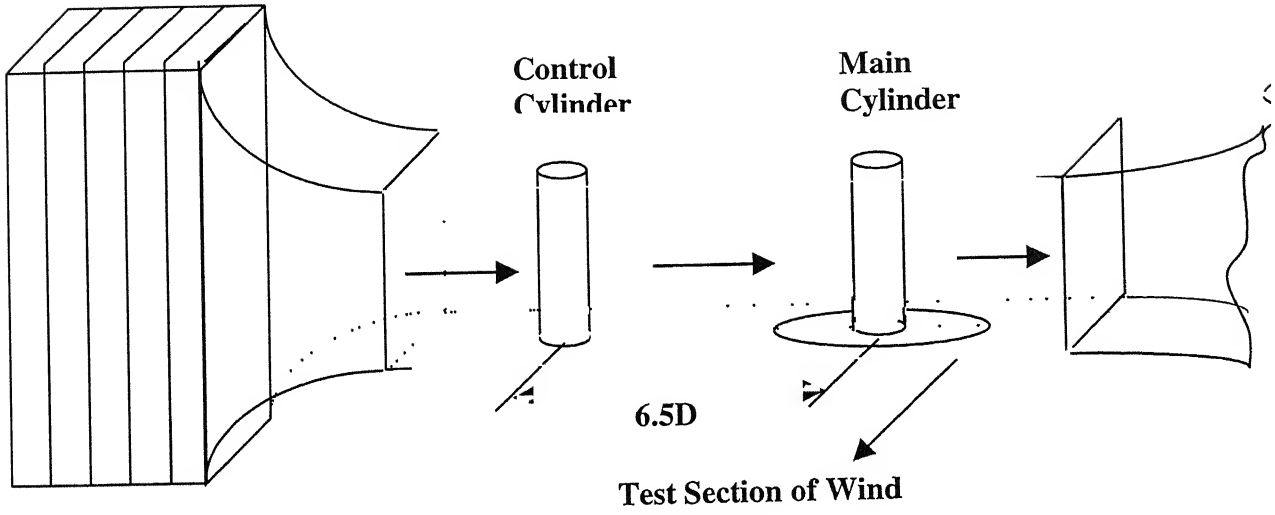

Figure 2. Relative Position of Two Cylinders

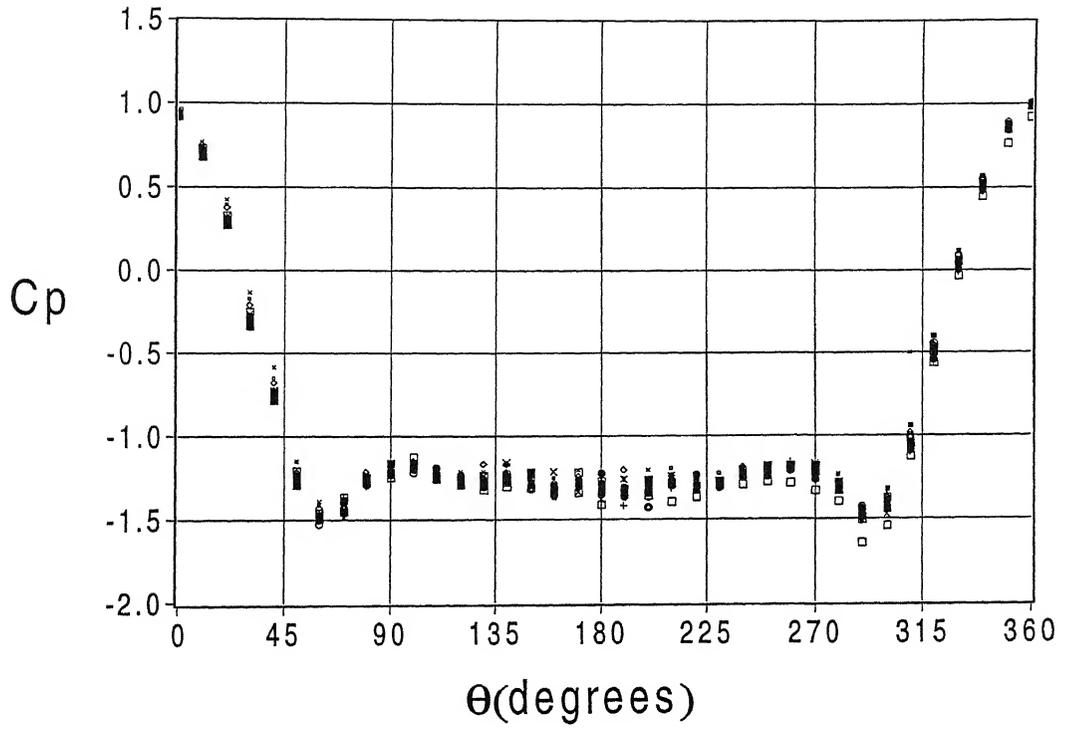

Figure 3(a) Variation of pressure with circumferential angle for Re = 13200 (without control cylinder); ▫, h/H=0.07; ●, h/H=0.13; ⊙, h/H=0.20; ■, h/H=0.27; ⊗, h/H=0.33; ⊡, h/H=0.40; ▪, h/H=0.47; +, h/H=0.53; +, h/H=0.60; ×, h/H=0.67; ×, h/H=0.73; ♦, h/H=0.80; ◘, h/H=0.87; ▪, h/H=0.93

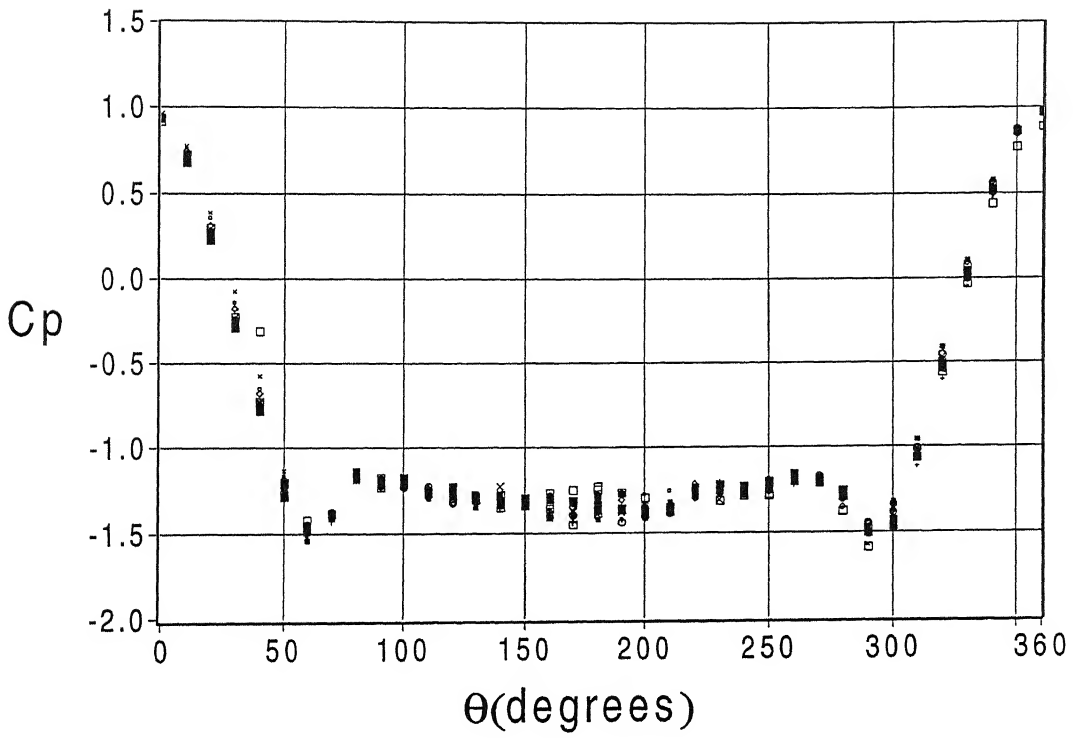

Figure 3(b) Variation of pressure with circumferential angle for Re = 19800 (without control cylinder); ▫, h/H=0.07; ●, h/H=0.13; ⊙, h/H=0.20; ■, h/H=0.27; ⊗, h/H=0.33; ⊡, h/H=0.40; ▪, h/H=0.47; +, h/H=0.53; +, h/H=0.60; ×, h/H=0.67; ×, h/H=0.73; ♦, h/H=0.80; ◘, h/H=0.87; ▪, h/H=0.93

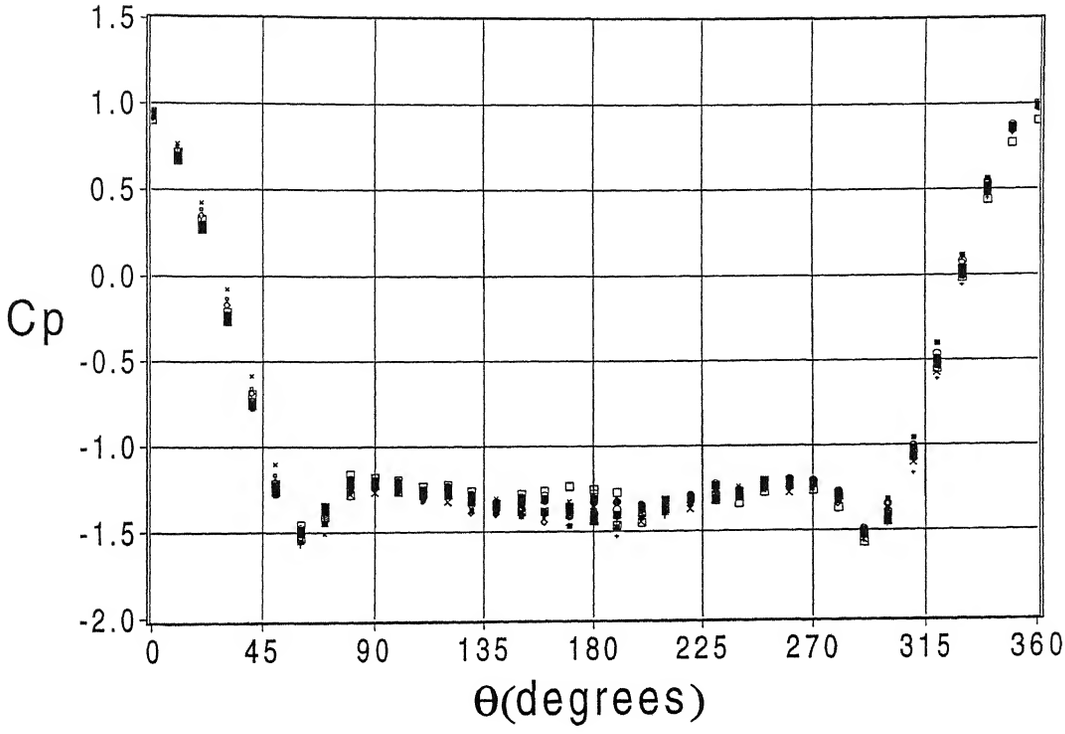

Figure 3(c) Variation of pressure with circumferential angle for Re = 26667 (without control cylinder); ▫, h/H=0.07; ●, h/H=0.13; ⊙, h/H=0.20; ■, h/H=0.27; ⊗, h/H=0.33; ⊡, h/H=0.40; ▪, h/H=0.47; +, h/H=0.53; +, h/H=0.60; ×, h/H=0.67; ×, h/H=0.73; ♦, h/H=0.80; ◘ , h/H=0.87; • , h/H=0.93

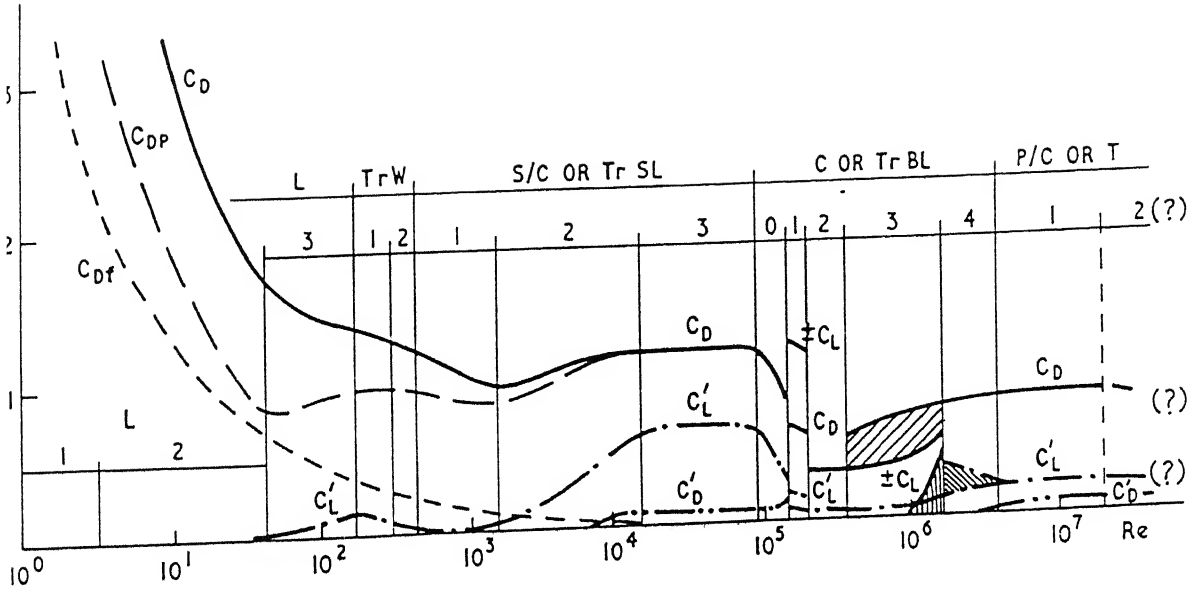

Figure 4. Variation of drag coefficient with Reynolds Number (Schlichting, H.)

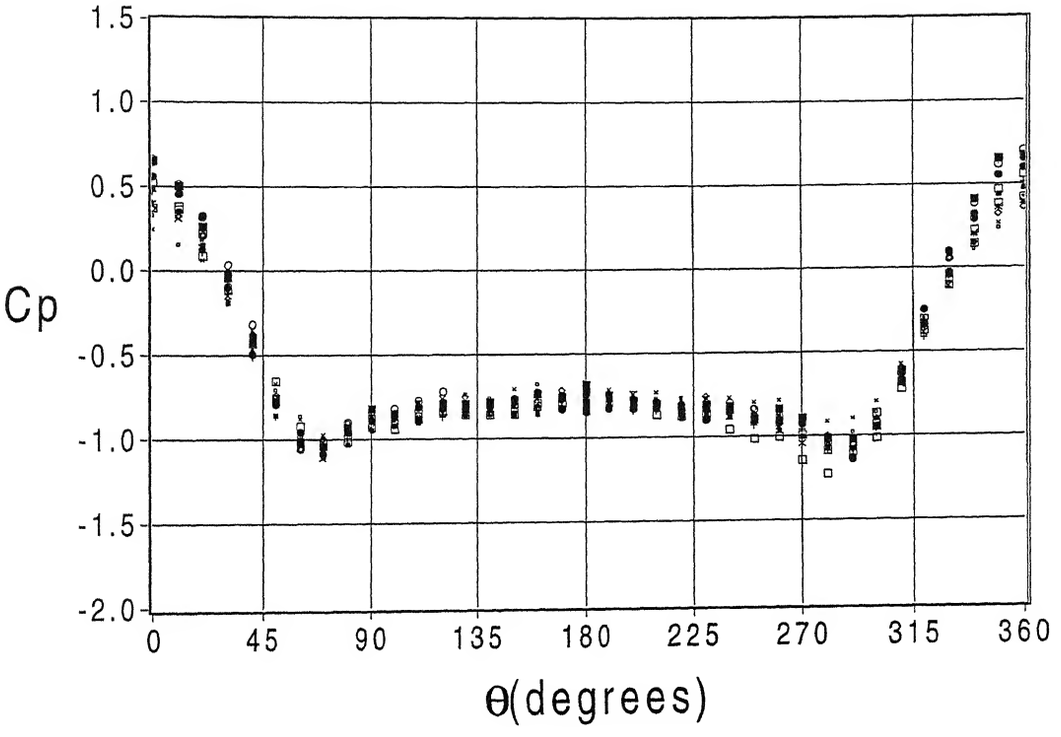

Figure 5(a) Variation of pressure with circumferential angle for Re = 13200 and ψ = 0°(tandem Arrangement); ▫, h/H=0.07; ●, h/H=0.13; ⊙, h/H=0.20;■, h/H=0.27; ⊗, h/H=0.33; ⊡, h/H=0.40; ▪, h/H=0.47; +, h/H=0.53; +, h/H=0.60; ×, h/H=0.67; ×, h/H=0.73; ♦, h/H=0.80; ◘, h/H=0.87; ▪, h/H=0.93

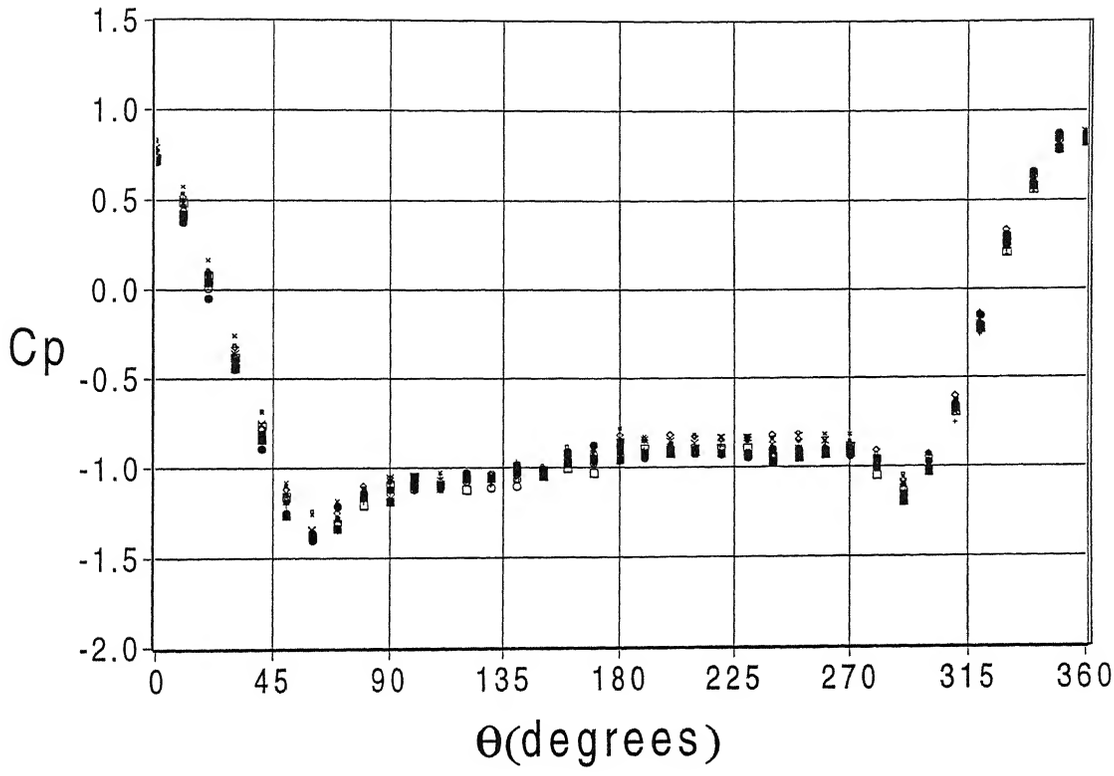

Figure 5(b) Variation of pressure with circumferential angle for Re = 13200 and $\psi = 10°$ (staggered arrangement); ▫, h/H=0.07; •, h/H=0.13; ⊙h/H=0.20;■ , h/H=0.27; ⊗, h/H=0.33; ⊡, h/H=0.40; ▪ , h/H=0.47; +, h/H=0.53; +, h/H=0.60; ×, h/H=0.67; ×, h/H=0.73; ♦, h/H=0.80; ◘ , h/H=0.87; ▪, h/H=0.93

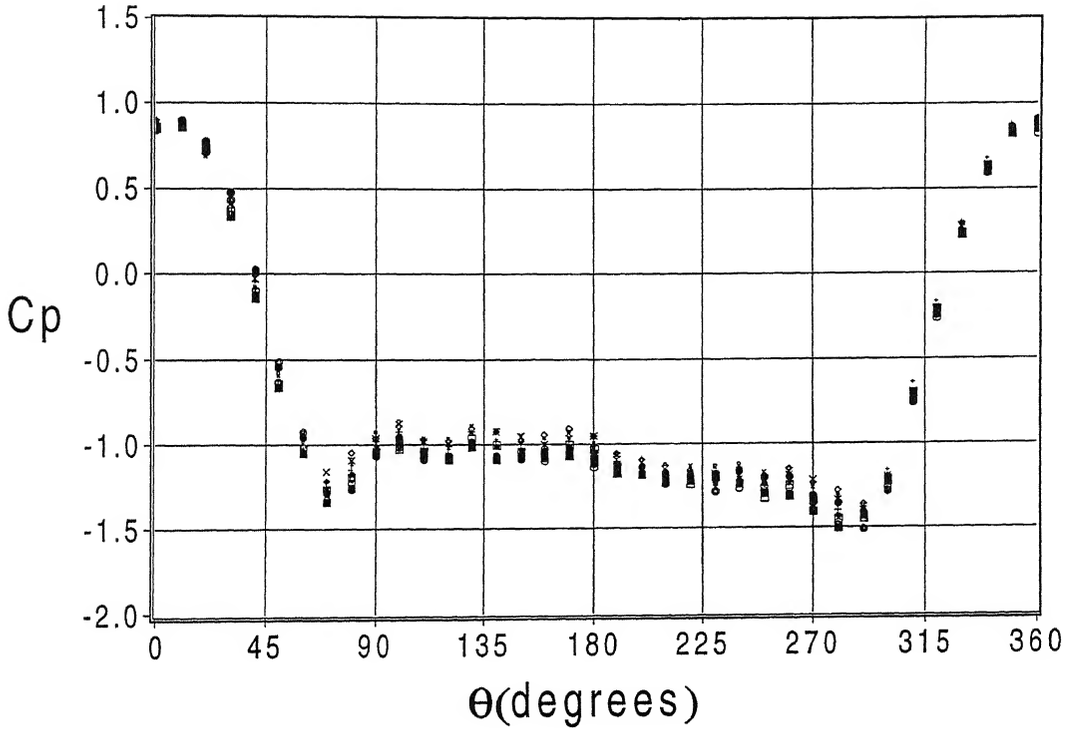

Figure 5(c) Variation of pressure with circumferential angle for Re = 13200 and ψ = -10° (staggered arrangement); ▫, h/H=0.07; •, h/H=0.13; ⊙h/H=0.20;■, h/H=0.27; ⊗, h/H=0.33; ⊡, h/H=0.40; ▪, h/H=0.47; +, h/H=0.53; +, h/H=0.60; ×, h/H=0.67; ×, h/H=0.73; ♦, h/H=0.80; ◘, h/H=0.87; ▪, h/H=0.93

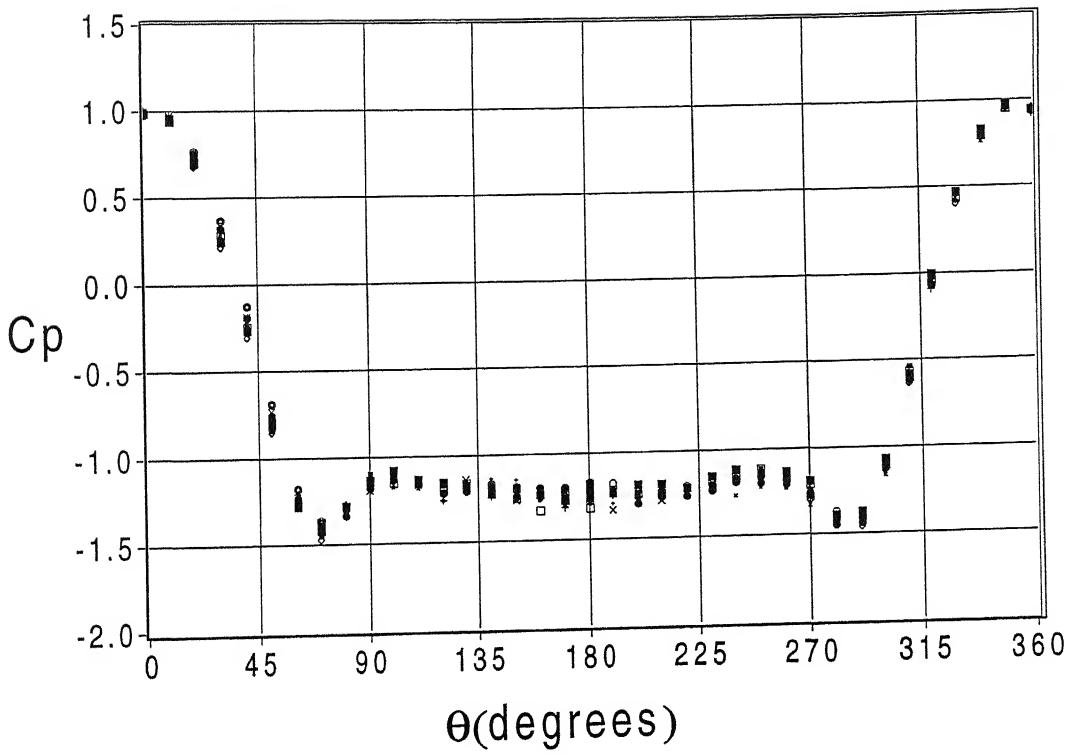

Figure 5(d) Variation of pressure with circumferential angle for Re = 13200 and ψ = -20° (staggered arrangement); ▫, h/H=0.07; •, h/H=0.13; ⊙, h/H=0.20;■, h/H=0.27; ⊗, h/H=0.33; ⊡, h/H=0.40; ▪, h/H=0.47; +, h/H=0.53; +, h/H=0.60; ×, h/H=0.67; ×, h/H=0.73; ♦, h/H=0.80; ◘, h/H=0.87; ·, h/H=0.93

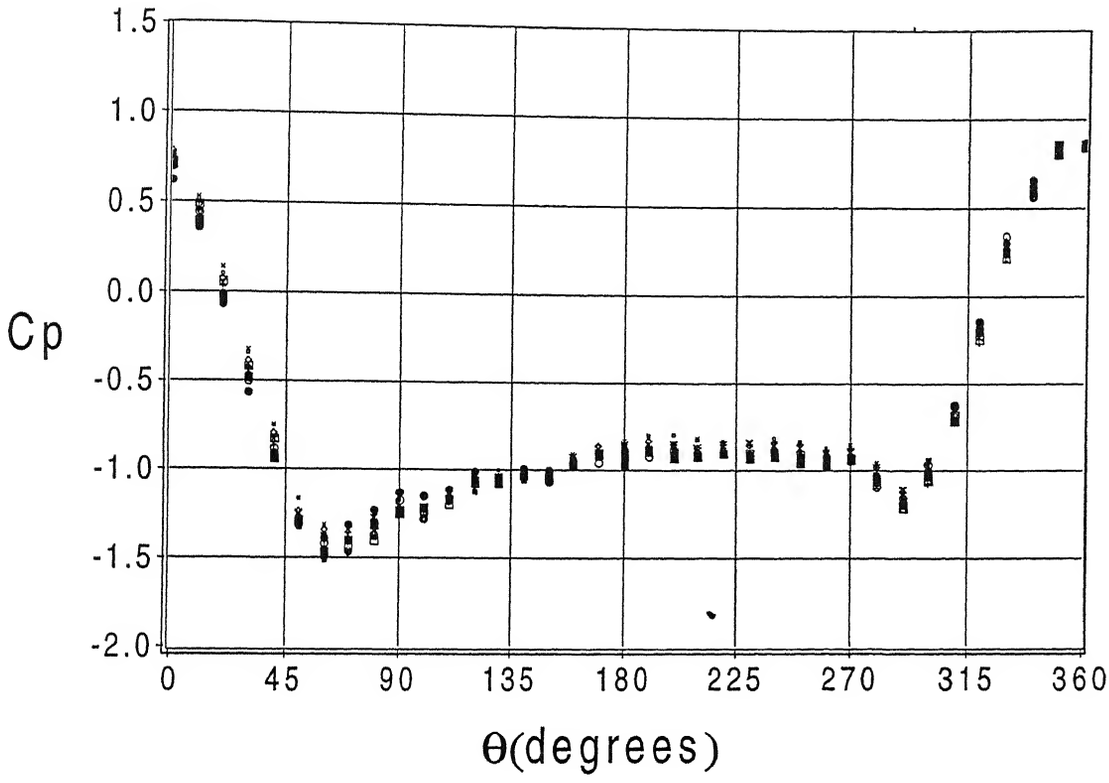

Figure 6(a) Variation of pressure with circumferential angle for Re = 19800 and $\psi = 10°$ (staggered arrangement); ▫, h/H=0.07; •, h/H=0.13; ⊙, h/H=0.20;■, h/H=0.27; ⊗, h/H=0.33; ⊡, h/H=0.40; ▪, h/H=0.47; +, h/H=0.53; +, h/H=0.60; ×, h/H=0.67; ×, h/H=0.73; ♦, h/H=0.80; ◘, h/H=0.87; ·, h/H=0.93

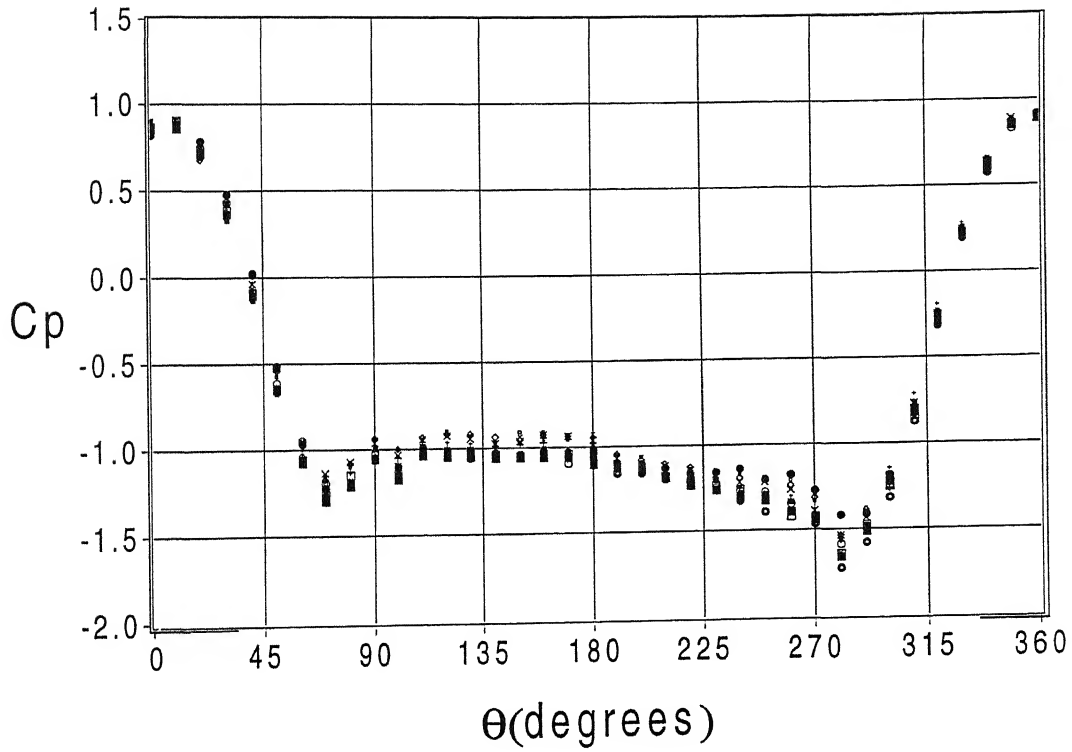

Figure 6(b) Variation of pressure with circumferential angle for Re = 19800 and $\psi = -10°$ (staggered arrangement); ▫, h/H=0.07; •, h/H=0.13; ⊙, h/H=0.20;■ , h/H=0.27; ⊗, h/H=0.33; ⊡, h/H=0.40; ▪, h/H=0.47; +, h/H=0.53; +, h/H=0.60; ×, h/H=0.67; ×, h/H=0.73; ♦, h/H=0.80; ◘ , h/H=0.87; ·, h/H=0.93

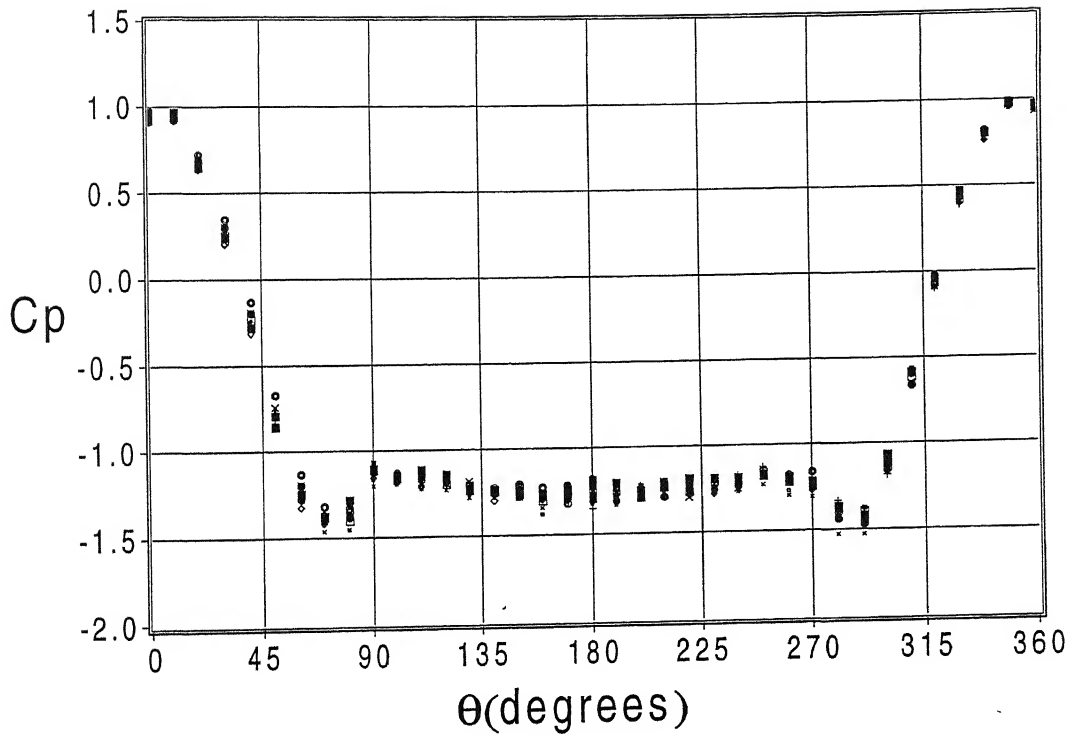

Figure 6(c) Variation of pressure with circumferential angle for Re = 19800 and ψ = -20° (staggered arrangement); ▫, h/H=0.07; •, h/H=0.13;⊙h/H=0.20; ■, h/H=0.27; ⊗, h/H=0.33; ⊡, h/H=0.40; ▪, h/H=0.47; +, h/H=0.53; +, h/H=0.60; ×, h/H=0.67; ×, h/H=0.73; ♦, h/H=0.80; ◘ , h/H=0.87; ⋆, h/H=0.93

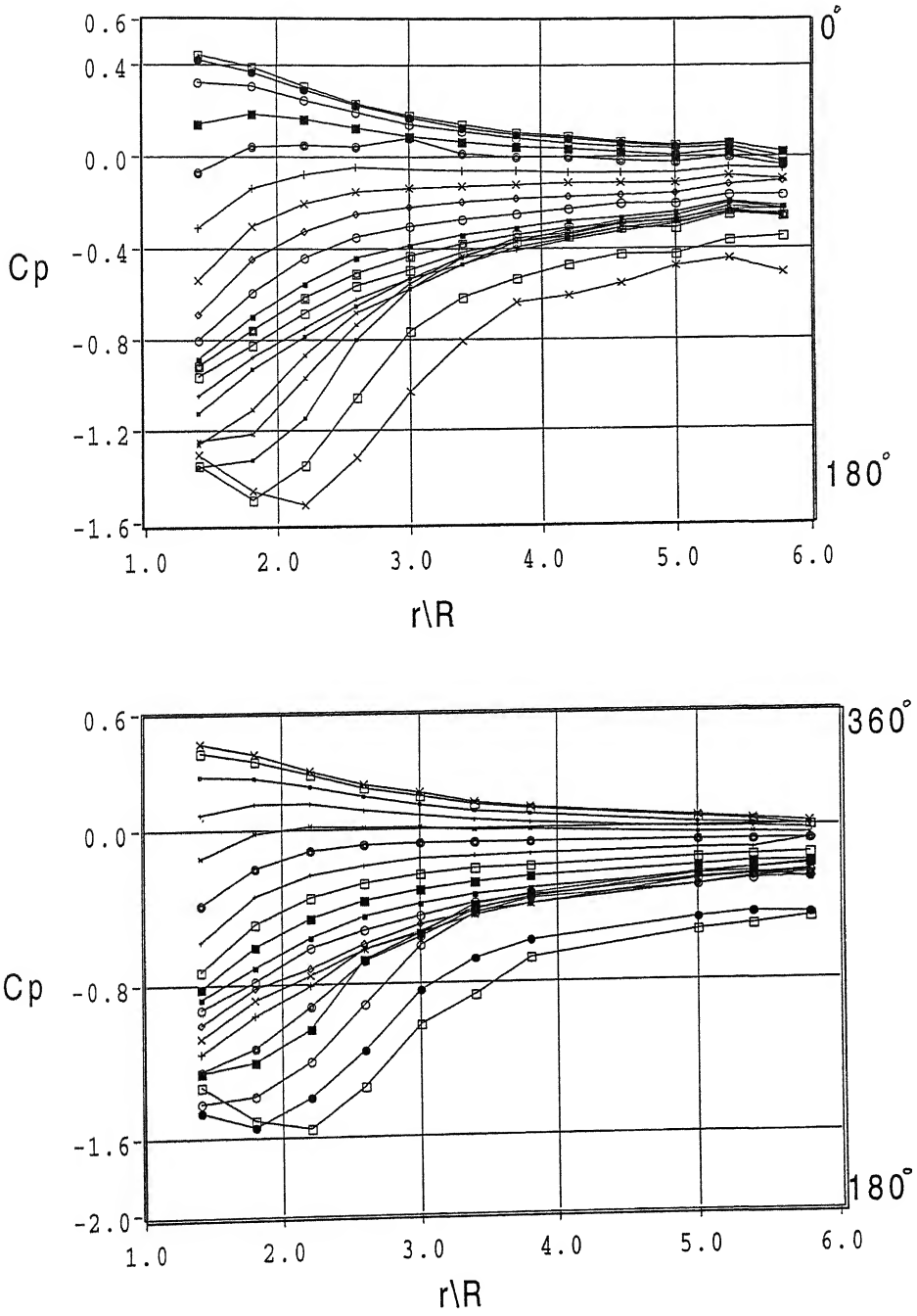

Figure 7(a) Variation of pressure with radial distance for Re = 26667 at various θ (without control cylinder); ▫, θ=0°, 360°; •, θ=10°,350°; ⊙, θ=20°,340°; ■,θ=30°, 330°; ⊙, θ=40°,320°; +,θ=50°,310°; ×, θ=60°,300°; ⋆,θ=70°,290°; ⊙, θ=80°,280°; ⋆, θ=90°,270°; ◘, θ=100°, 260°; +, θ=110°, 250°; ⋆, θ=120°, 240°; ×,θ=130°, 230°; •,θ=140°, 220°; ⊡, θ=150°, 210°; ×, θ=160°, 200°; ◘, θ=170°, 190°; •,θ=180°, 180°

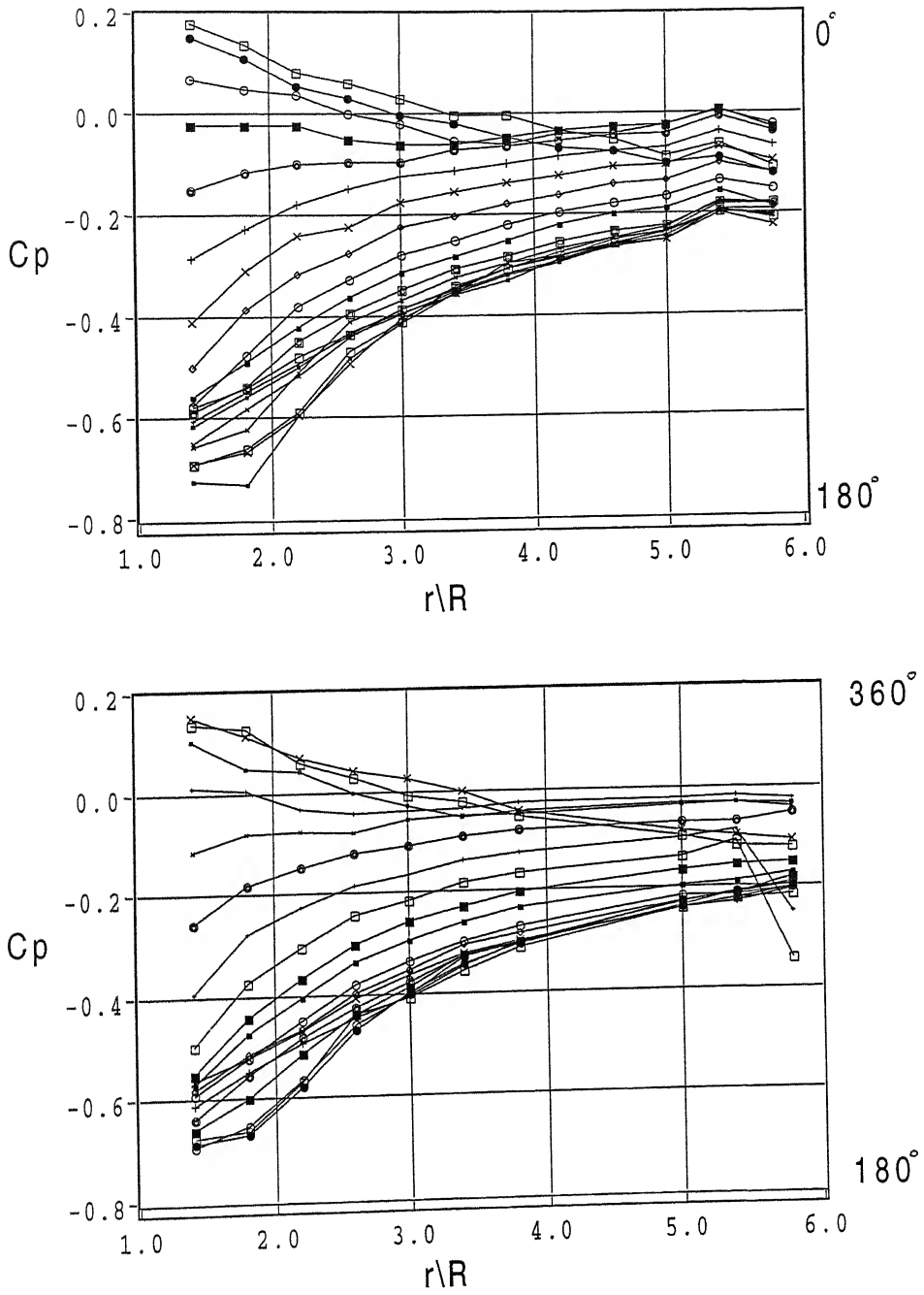

Figure 7(b) Variation of pressure with radial distance for Re = 19800 and ψ = 0° at various θ (tandem arrangement); ▫, θ=0°, 360°; ●, θ=10°, 350°; o, θ=20°, 340°; ■,θ=30°, 330°; ⊙, θ=40°, 320°; +,θ=50°, 310°; ×, θ=60°, 300°; ⋆,θ=70°, 290°; ⊙, θ=80°, 280°; ⋆, θ=90°, 270°; ▫, θ=100°, 260°; +, θ=110°, 250°; ⋆, θ=120°, 240°; ×,θ=130°, 230°; •,θ=140°, 220°; ⊡, θ=150°, 210°; ×, θ=160°, 200°; ▫, θ=170°, 190°; ●, θ=180°, 180°

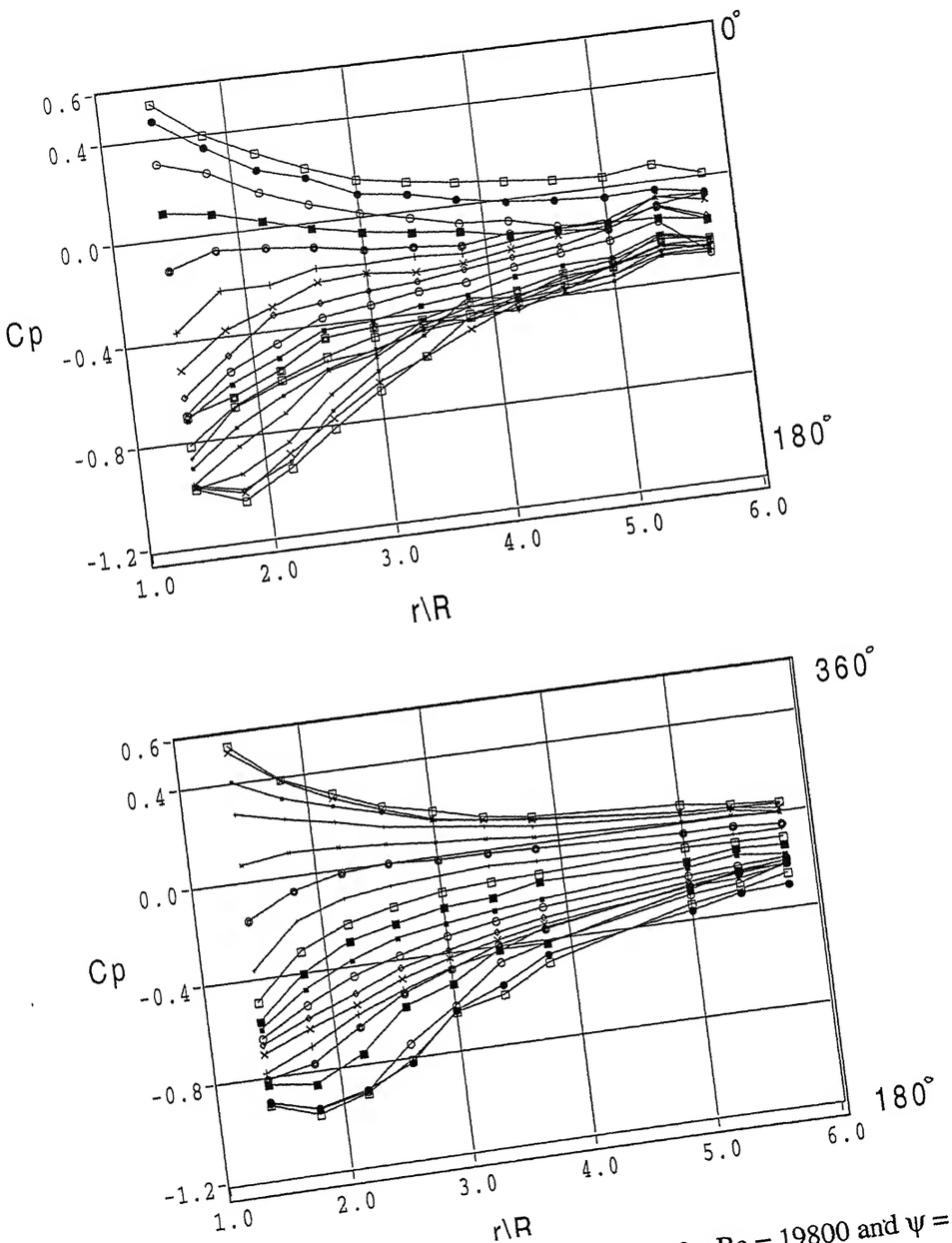

Figure 7(c) Variation of pressure with radial distance for Re = 19800 and $\psi = 10°$ at various θ (staggered arrangement); ▫, θ=0°, 360°; ●, θ=10°, 350°; o, θ=20°, 340°; ■,θ=30°, 330°; ⊙, θ=40°, 320°; +,θ=50°, 310°; ×, θ=60°, 300°; ⋆, θ=70°, 290°; ⊙, θ=80°, 280°; ⋆, θ=90°, 270°; ▫, θ=100°, 260°; +, θ=110°, 250°; ⋆, θ=120°, 240°; ×,θ=130°, 230°; •,θ=140°, 220°; ⊡, θ=150°, 210°; ×, θ=160°, 200°; ▫, θ=170°, 190°; ●, θ=180°, 180°

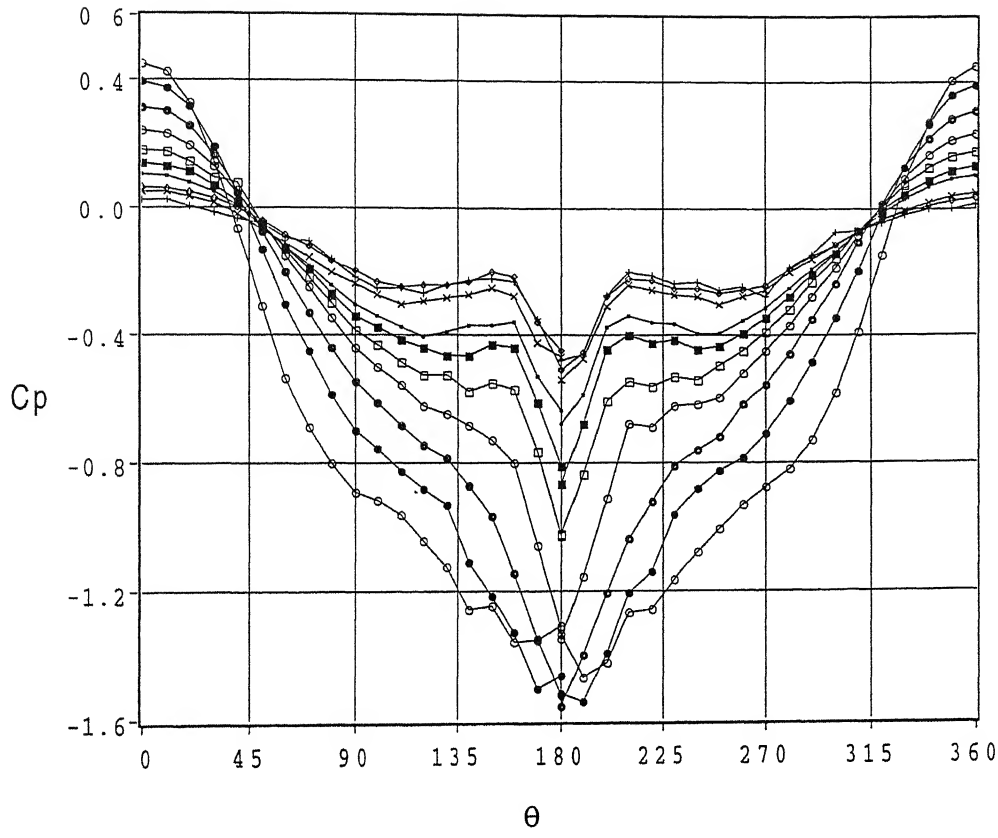

Figure 8(a) Variation of pressure with circumferertial angle at different radial distances for Re = 26667 (without control cylinder); o, r/R=1.4; •, r/R=1.8; ⊗, r/R=2.2; ⊙, r/R=3.0; ▫, r/R=3.4; ▪, r/R=3.8; ▪, r/R=5.0; ×, r/R=5.4; ⋆, r/R=5.8

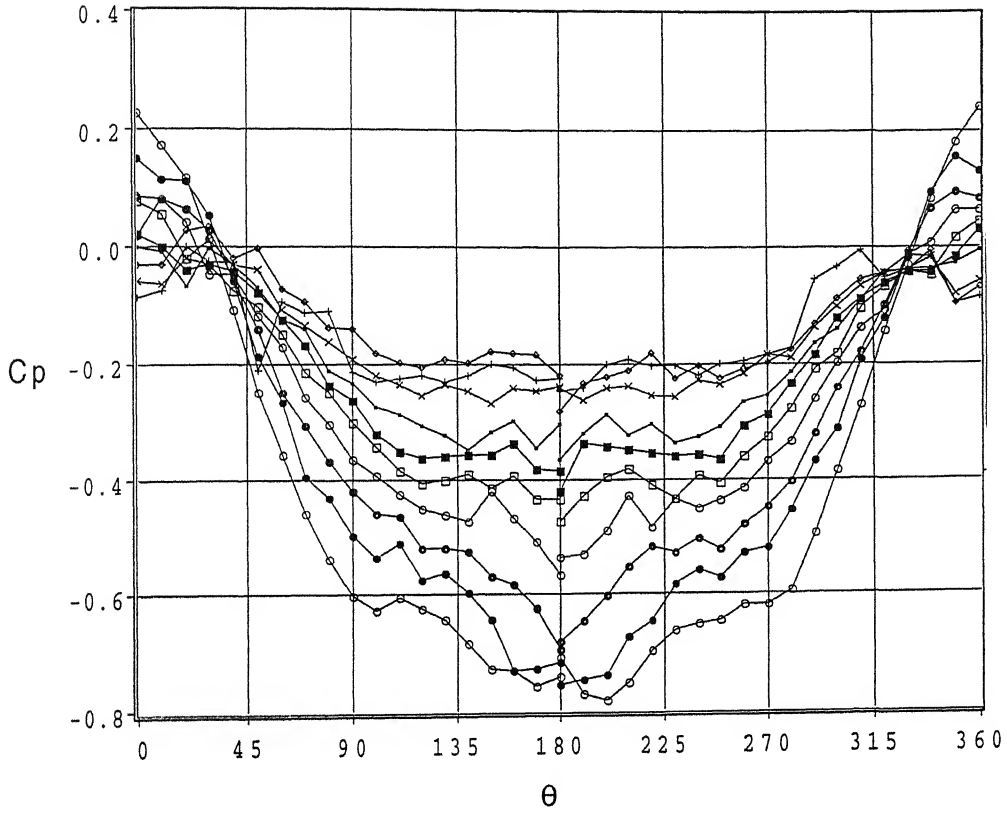

Figure 8(b) Variation of pressure with circumferertial angle at different radial distances for Re =13200 and $\psi = 0°$ (tandem arrangement); o, r/R=1.4; •, r/R=1.8; ⊗, r/R=2.2; ⊙, r/R=3.0; ▫, r/R=3.4; ■, r/R=3.8; ▪, r/R=5.0; ×, r/R=5.4; ⬩, r/R=5.8

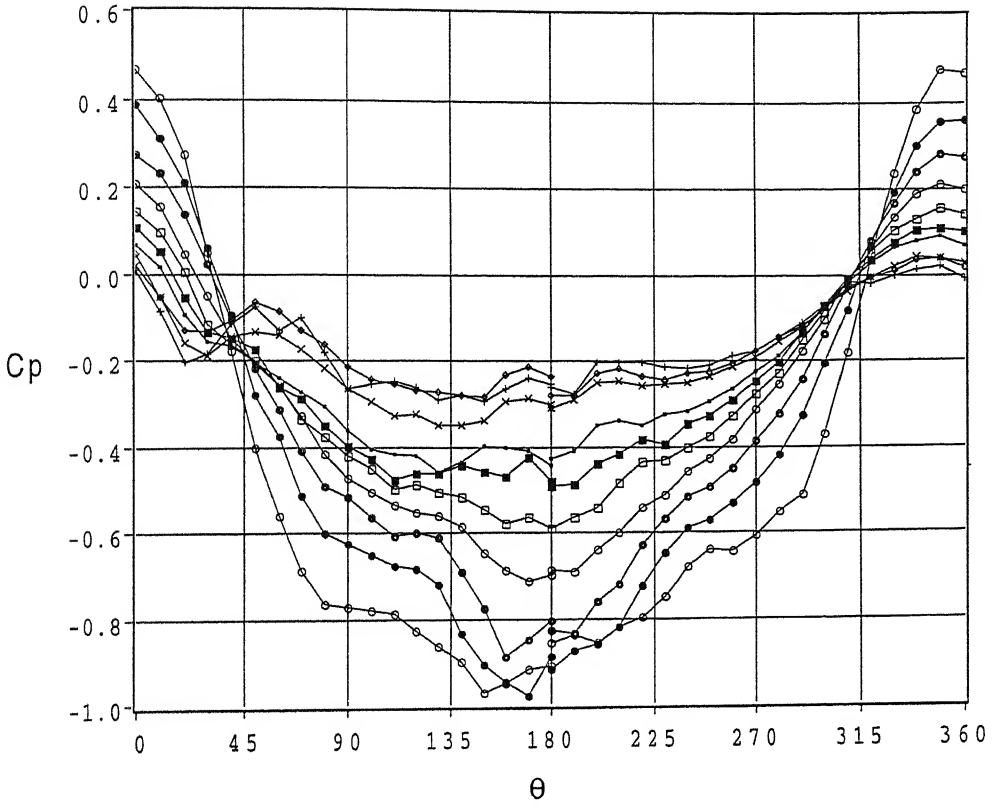

Figure 8(c) Variation of pressure with circumferertial angle at different radial distances for Re =19800 and $\psi = 10°$ (staggered arrangement)

o, r/R=1.4; •, r/R=1.8; ⊗, r/R=2.2; ⊙, r/R=3.0; □, r/R=3.4; ■, r/R=3.8; ▪, r/R=5.0; ×, r/R=5.4; ⋆, r/R=5.8

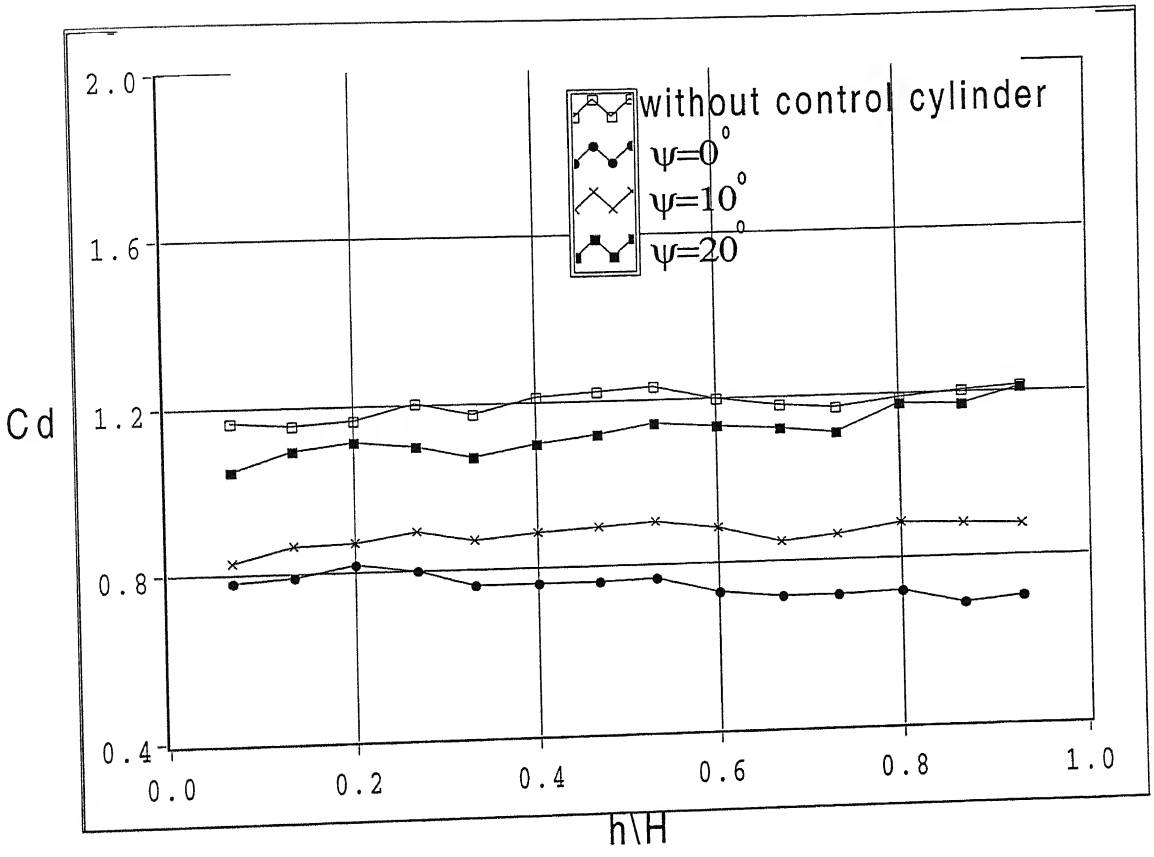

Figure 9 Variation of drag coefficient with height

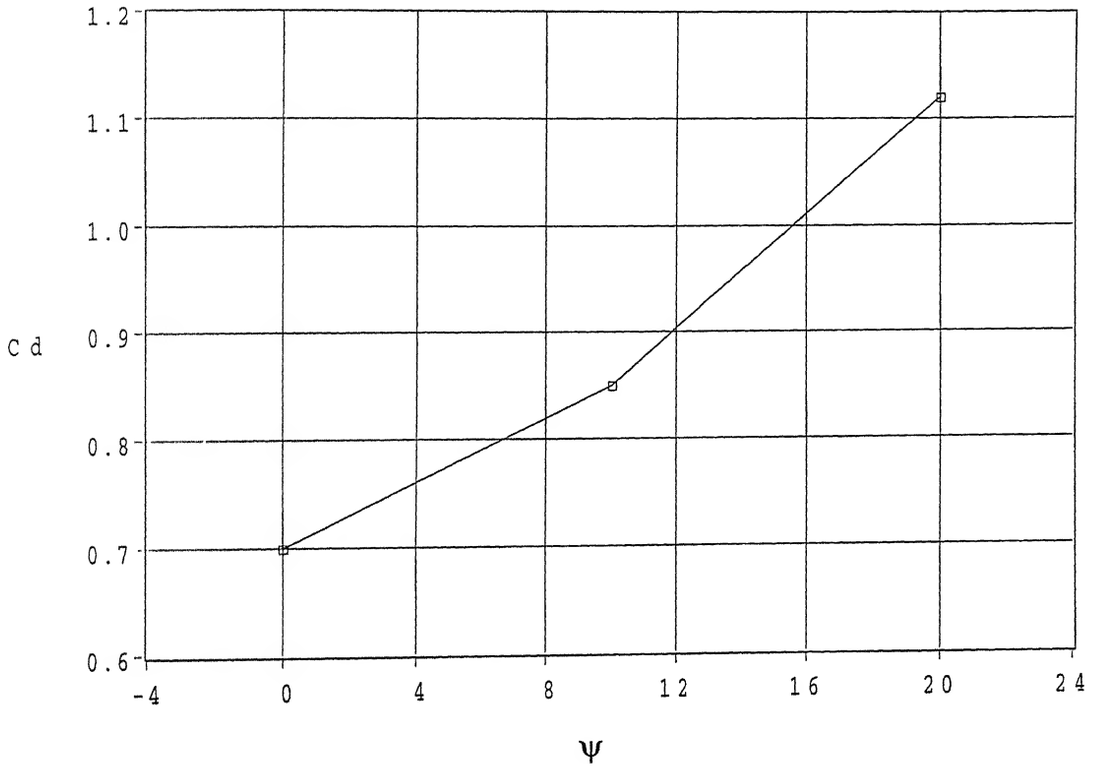

Figure 10 Variation of drag coefficient with stagger angle

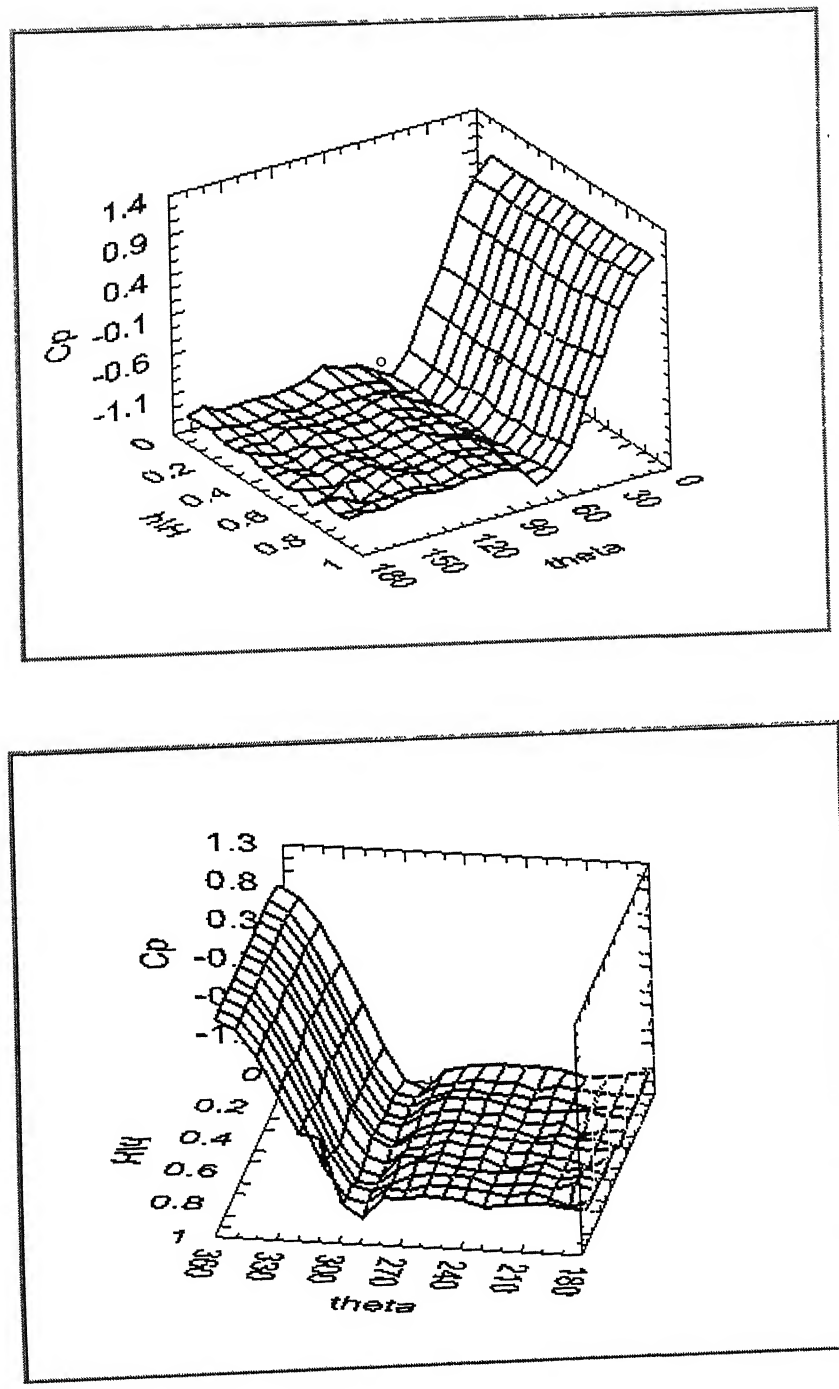

Figure 11(a) Variation of pressure with circumferential angle at different heights for Re = 13200 (surface plot) (without control cylinder)

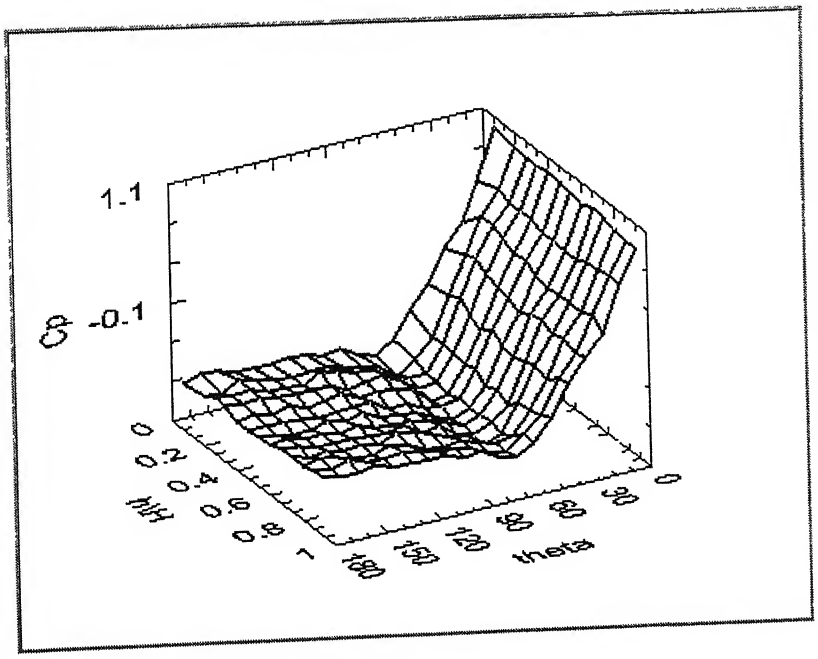

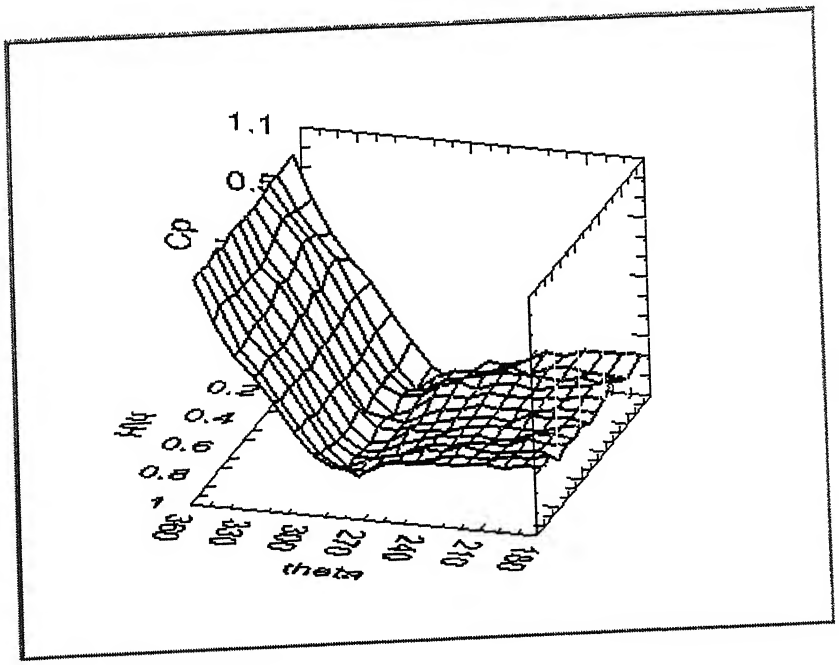

Figure 11(b) Variation of pressure with circumferential angle at different heights for Re = 13200 and $\psi = 0°$ (surface plot)

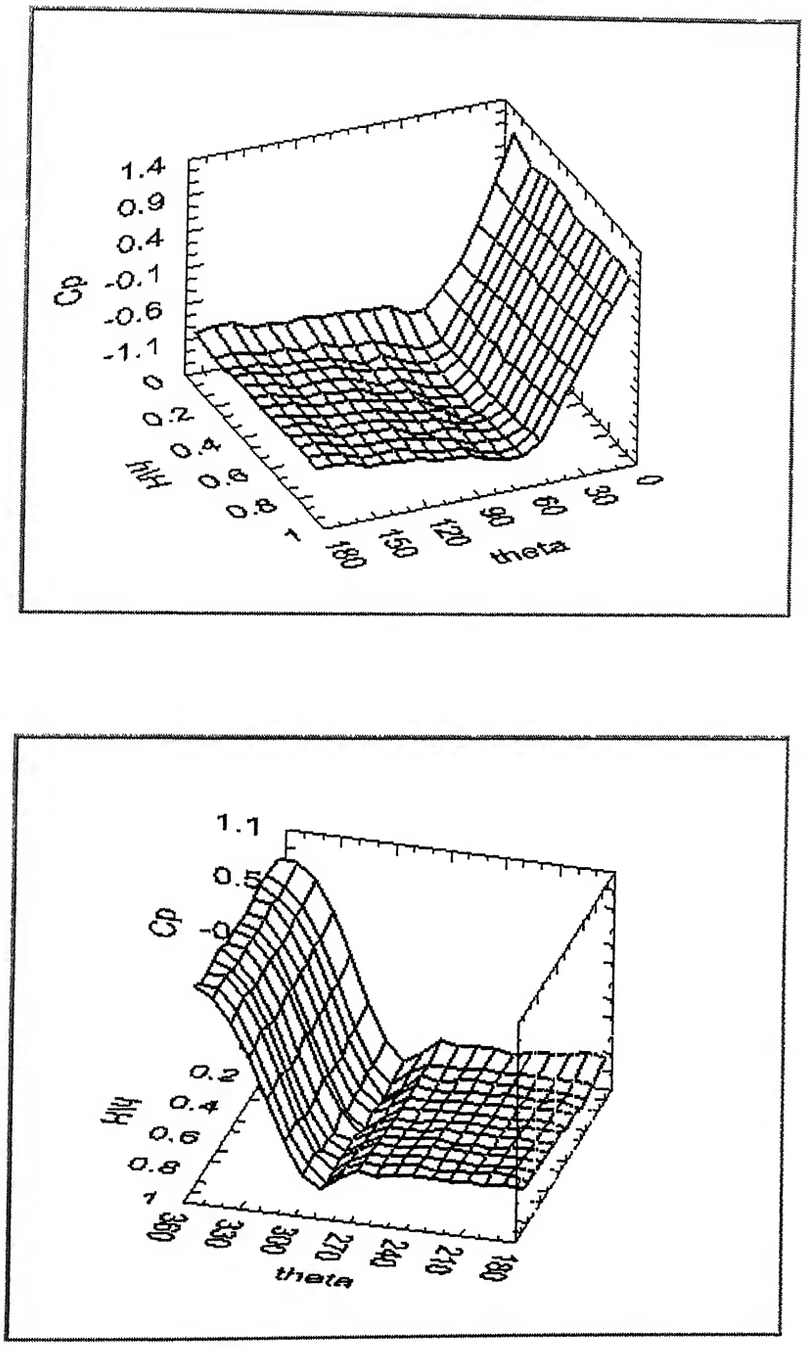

Figure 11(c) Variation of pressure with circumferential angle at different heights
Re = 19800 and $\psi = 10°$ (surface plot)

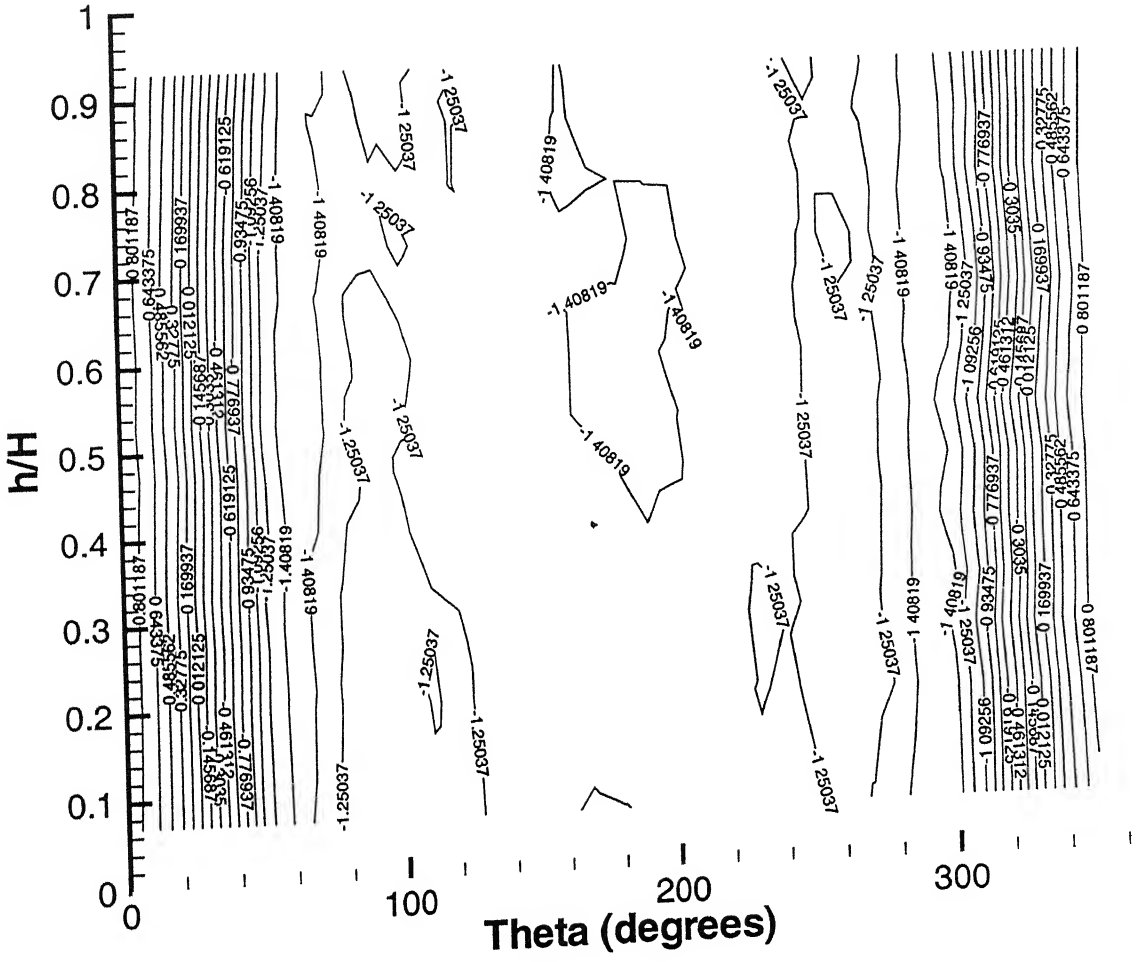

Figure 12(a) Pressure distribution on the surface of the cylinder at Re = 26667 (without control cylinder)

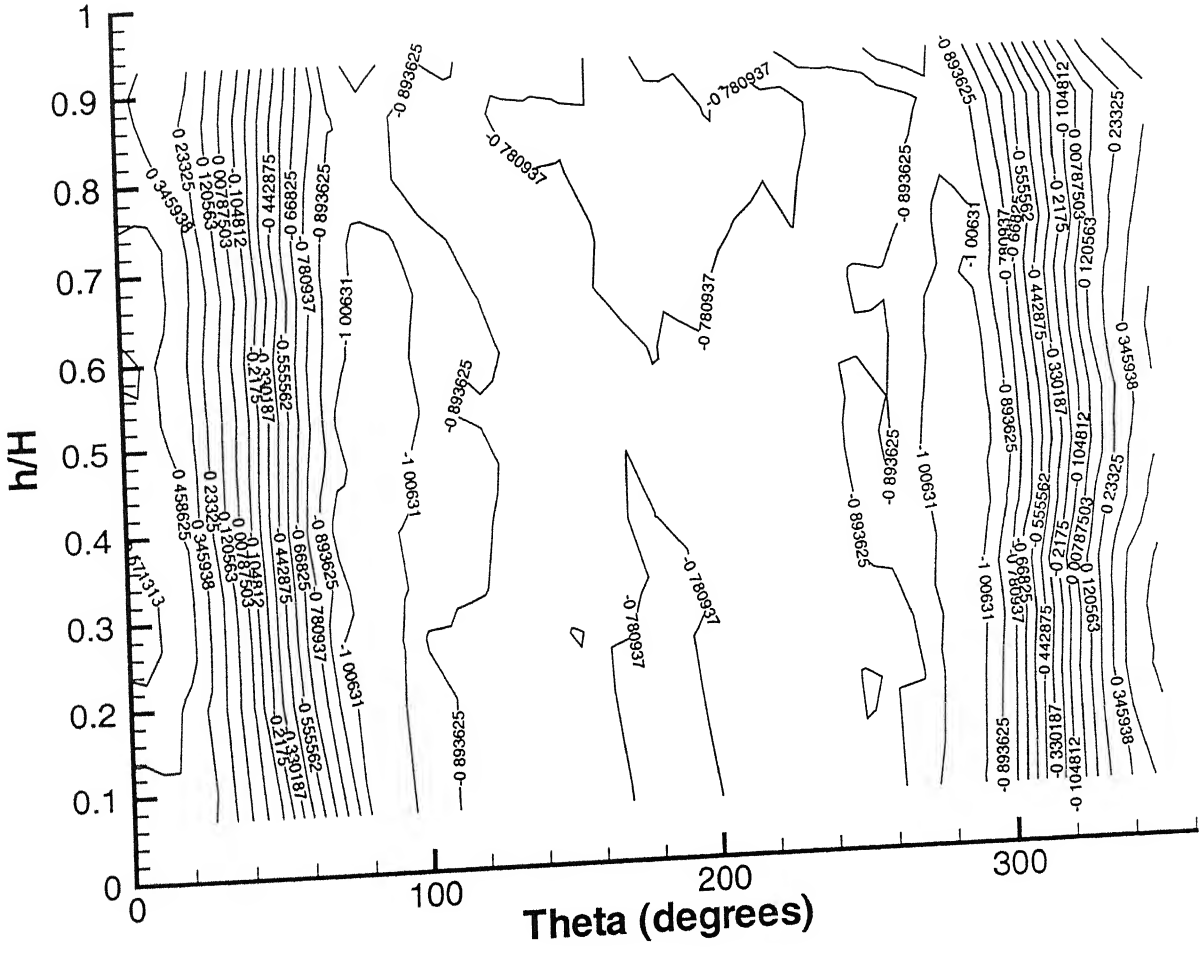

Figure 12(b) Pressure distribution on the surface of the cylinder at Re = 13200 and $\psi = 0°$

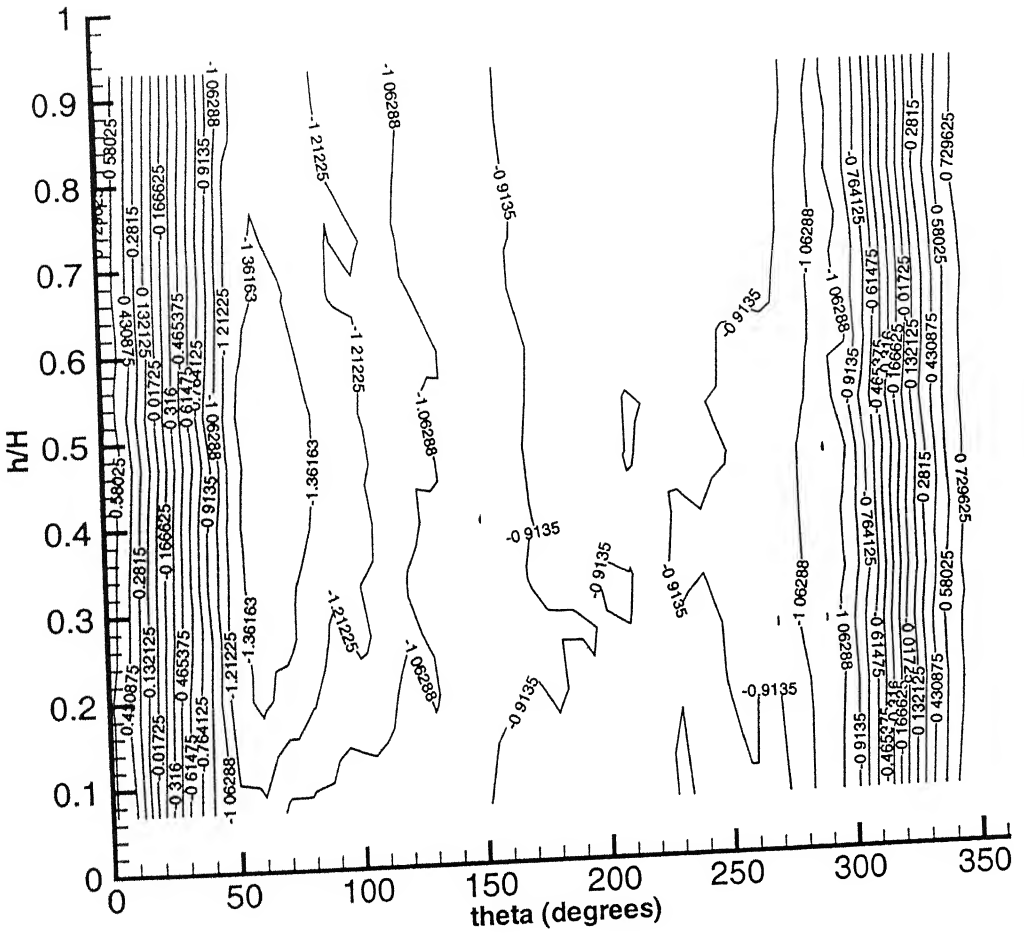

Figure 12(c) Pressure distribution on the surface of the cylinder at Re = 19800 and $\psi = 10$

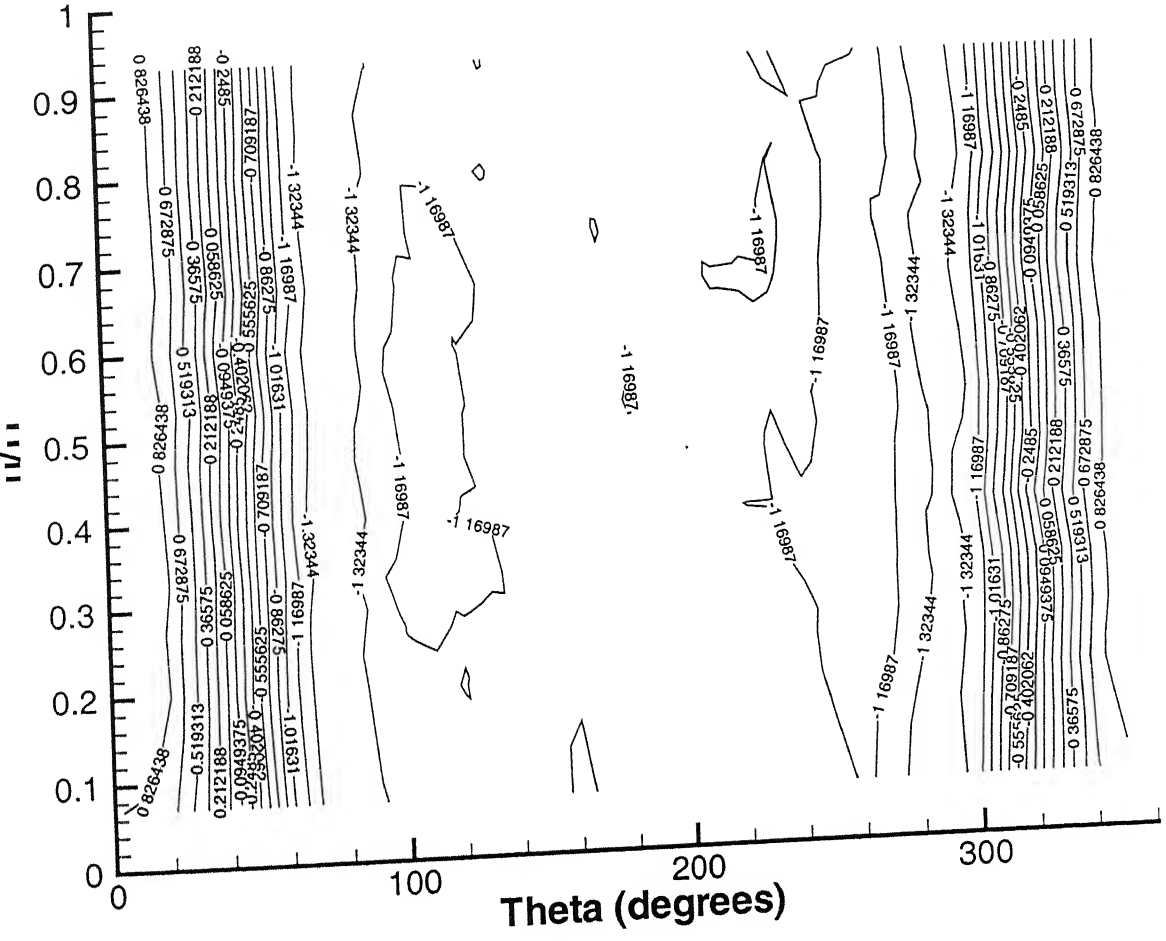

Figure 12(d) Pressure distribution on the surface of the cylinder at Re = 13200 and $\psi = 20°$

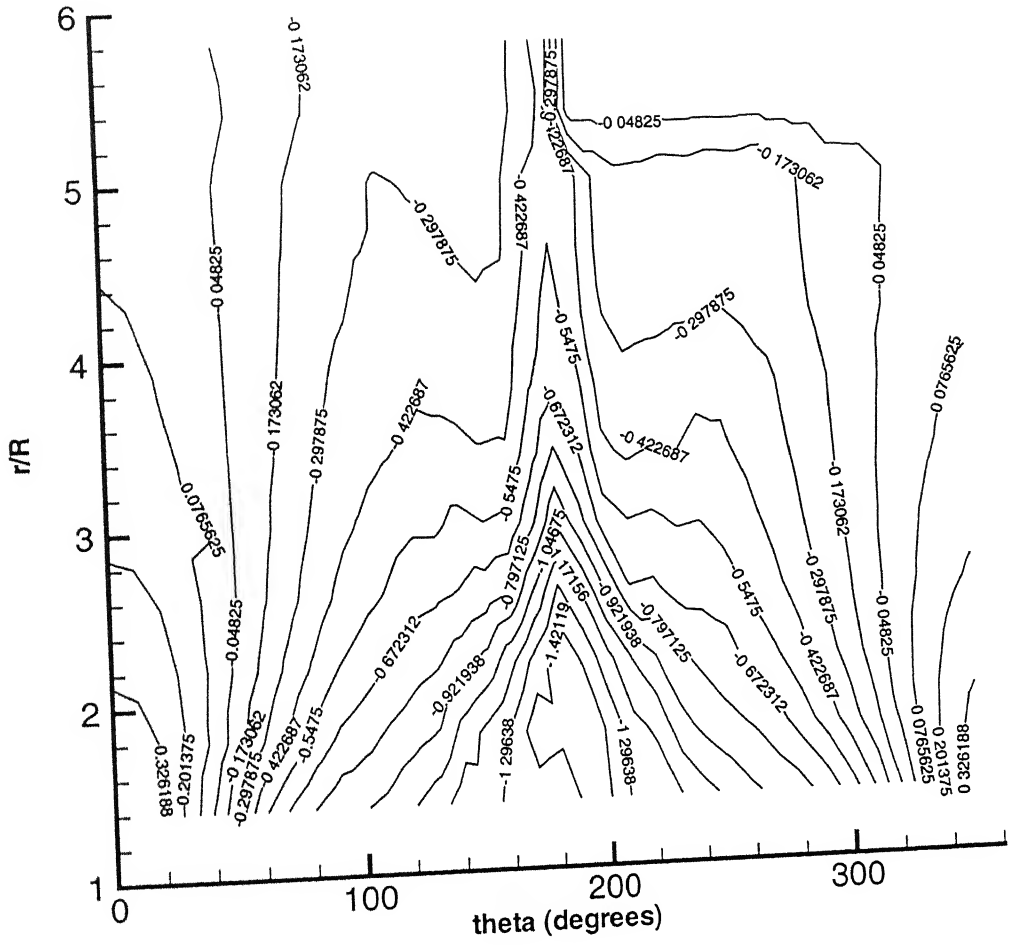

Figure 12(c) Pressure distribution on the surface of the disc around the cylinder at Re = 26667 (without control cylinder)

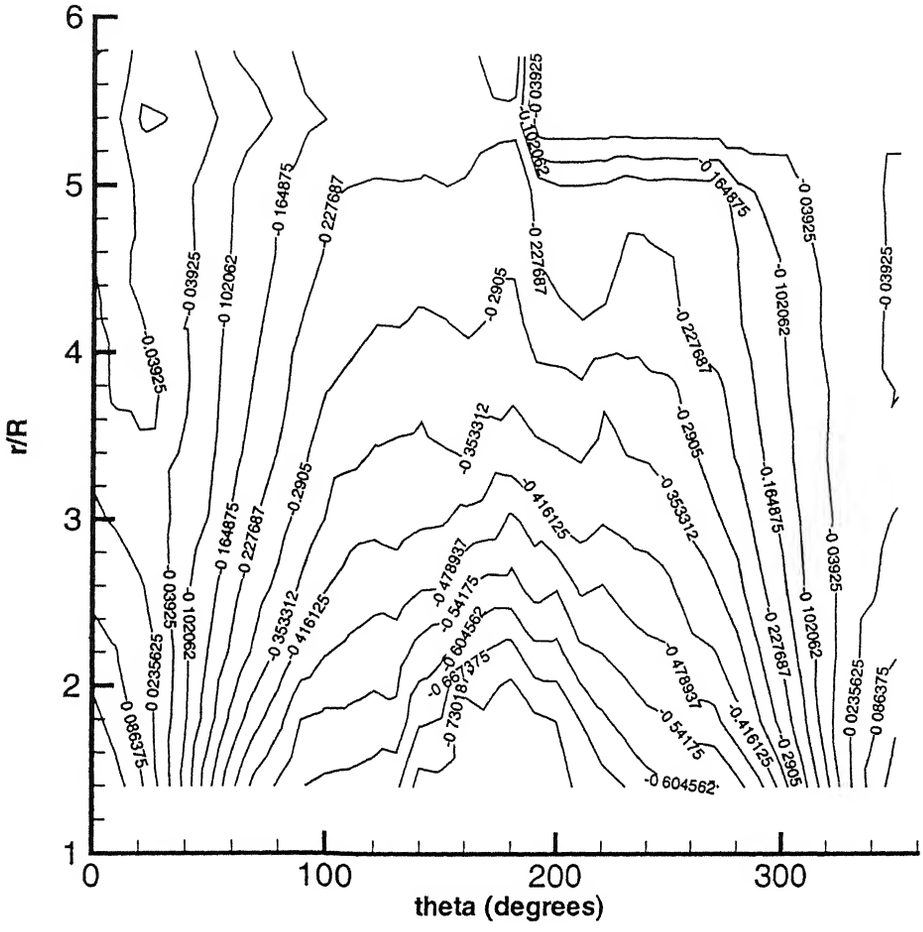

Figure12(f) Pressure distribution on the surface of the plate disc around the cylinder at Re = 13200 and $\psi = 0°$

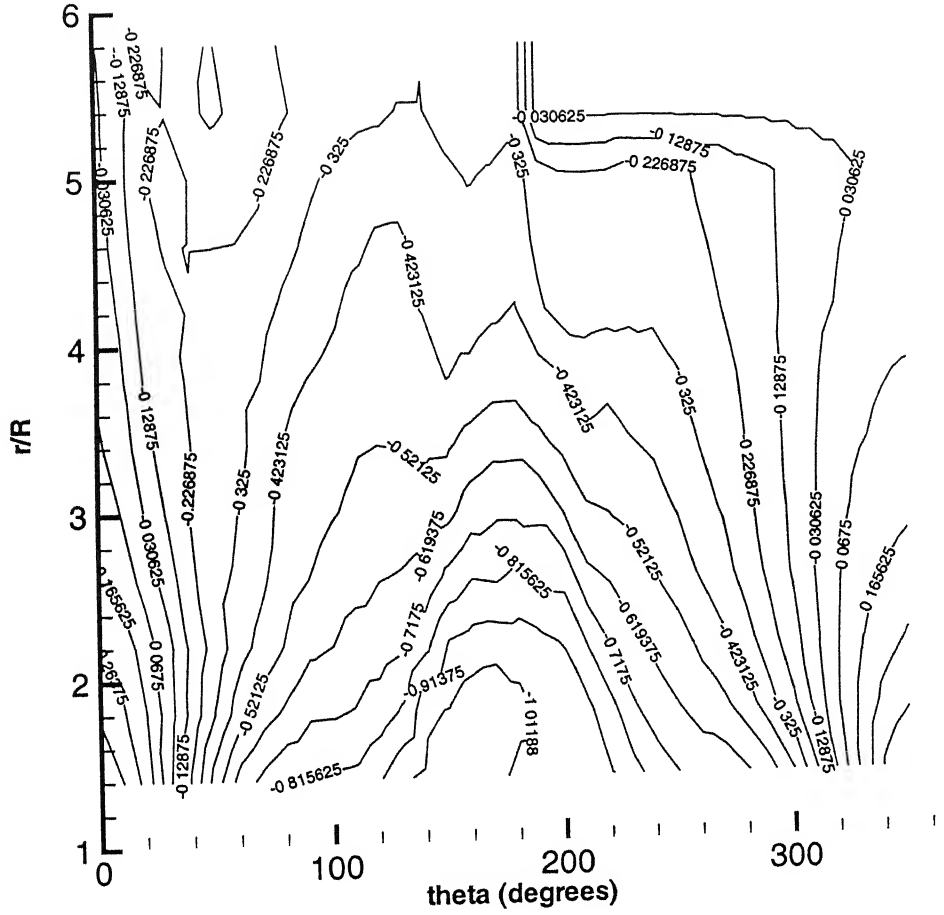

Figure 12(g) Pressure distribution on the surface of the disc around the cylinder at Re = 19800 and $\psi = 10°$

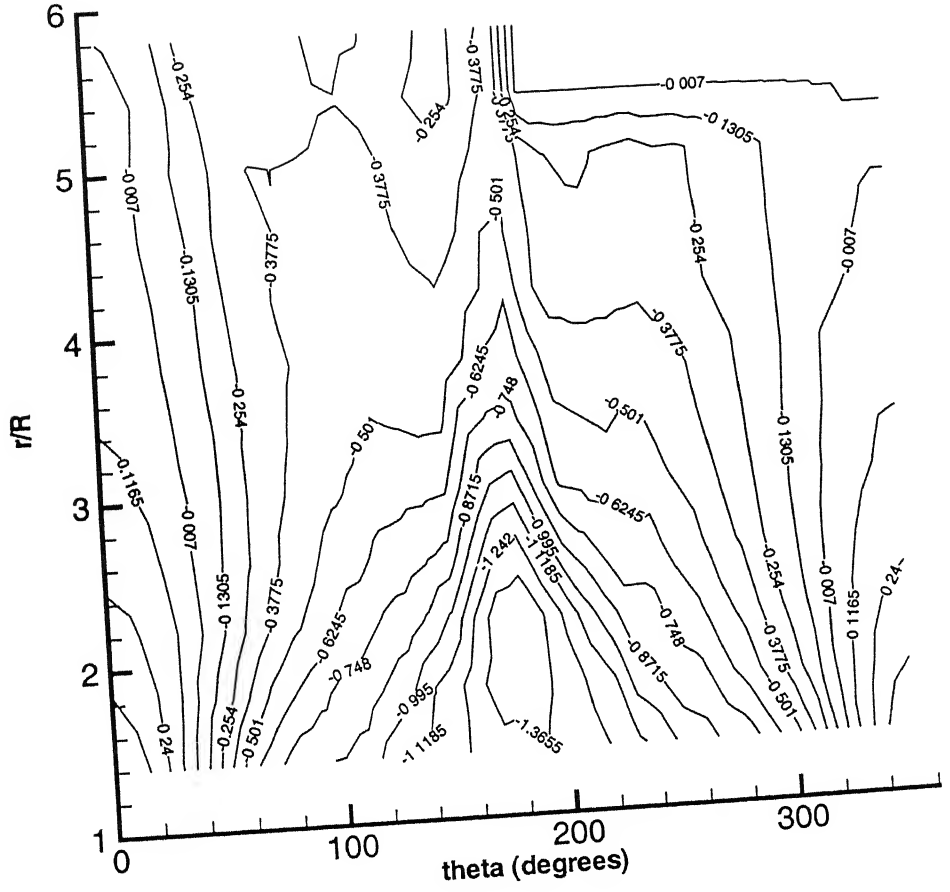

Figure 12(h) Pressure distribution on the surface of the disc around the cylinder at Re = 13200 and $\psi = 20°$

133626

Date Slip